Recycling an uplifted early foreland basin fill: an example from the Jaca basin (Southern Pyrenees, Spain)

M. Roigé[1*], D. Gómez-Gras[1], E. Remacha[1], S. Boya[1], M. Viaplana-Muzas[2], A. Teixell[1]

[1]Departament de Geologia, Universitat Autònoma de Barcelona, 08193 Bellaterra, Spain (E-mail: roige.marta@gmail.com)

[2]Institute of Earth Sciences Jaume Almera (ICTJA-CSIC), Lluís Solé i Sabarís s/n, 08028 Barcelona, Spain (E-mail: marc.via.mu@gmail.com)

(*) Corresponding author

ABSTRACT

In the northern Jaca basin (Southern Pyrenees), the replacement of deep-marine by terrestrial environments during the Eocene records a main drainage reorganization in the active Pyrenean pro-wedge, which leads to recycling of earlier foreland basin sediments. The onset of late Eocene-Oligocene terrestrial sedimentation is represented by four main alluvial fans: Santa Orosia, Canciás, Peña Oroel and San Juan de la Peña, which appear diachronously from east to west. These alluvial fans are the youngest preserved sediments deposited in the basin. We provide new data on sediment composition and sources for the late Eocene-Oligocene alluvial fans and precursor deltas of the Jaca basin. Sandstone petrography allows identification of the interplay of axially-fed sediments from the east with transversely-fed sediments from the north. Compositional data for the alluvial fans reflects a dominating proportion of recycled rock fragments derived from the erosion of a lower to middle Eocene flysch depocentre (the Hecho Group), located inmediately to the north. In addition, pebble composition allows identification of a source in the North Pyrenean Zone that provided lithologies from the Cretaceous carbonate flysch, Jurassic dolostones and Triassic dolerites. Thus we infer this zone as part of the source area, located in the headwaters, which would have been unroofed from turbidite deposits

during the late Eocene-Oligocene. These conclusions provide new insights on the response of drainage networks to uplift and topographic growth of the Pyrenees, where the water divide migrated southwards to its present day location.

KEYWORDS: sediment sources; Pyrenees; Jaca basin; recycling; alluvial fans; provenance

1. INTRODUCTION

Sediment recycling is a common process in foreland basins, where large volumes of syntectonic sediments can be reworked and reincoporated in younger deposits (Barone et al., 2008; Schlunegger and Mosar, 2011; Orts et al., 2012; Garzanti et al., 2013). Characterization of this process gives insights into the tectonic evolution and the erosional history of the source areas (Graham et al., 1986; Fosdick et al., 2015). However, in complex geodynamic settings, reliable criteria to identify detritus derived directly from basement rocks (igneous or metamorphic) or recycled from clastic rocks are scarce (Garzanti et al., 2013). In order to assess this problem, integration of various provenance sedimentary methods can provide valuable information about the nature of the source regions (Suttner, 1974; Dickinson, 1988).

In the southern Pyrenees, the Jaca foreland basin records the abandonment of turbiditic sedimentation (Hecho Group) during the late Eocene, followed by deltaic sedimentation that ends up with the terrestrial deposits of the Campodarbe Group (Puigdefàbregas, 1975). This transition is characterised by the progressive replacemement of the axially-fed sediments (eastern sources) that dominated during the deep-marine sedimentation, by transverse-fed sediments (northern, hinterland sources) represented by thick conglomerate acummulations in the northern margin of the Jaca basin. This occurred at a key stage of the basin evolution, when its western connection with the Atlantic ocean was interrupted during the Priabonian, and the

basin became internally drained (Puigdefàbregas, 1975; Hogan and Burbank, 1996; Costa et al., 2010).

In this work we apply sandstone petrography coupled with pebble point counting in order to provide new data on sediment composition and provenance of the last deltaic and fluvio-alluvial deposits of the Jaca basin. We analyse the main four alluvial fans of the northern margin of the basin, known as Santa Orosia, Canciás, Peña Oroel and San Juan de la Peña fans, which record the emersion of the former turbiditic basin due to activity of the Gavarnie thrust (Puigdefàbregas, 1975; Teixell, 1996; Roigé et al., 2016). Deposition of these sedimentary systems occurs while the northern active margin and folding structures emerging within the basin controlled sediment dispersal patterns and sediment routing systems. The main aim of this study is to define the sediment system response to the creation of new drainage patterns, and the major paleogeographic reorganization that took place during the uplift and topographic growth of the west-central Pyrenees.

2. GEOLOGICAL SETTING

2.1 Geological and stratigraphic framework

The Pyrenees are an alpine mountain belt that resulted from the collision between the Eurasian and Iberian plates during the late Cretaceous-early Miocene (Roure et al., 1989; Muñoz, 1992; Teixell, 1998; Vergés et al., 2002; Mouthereau et al., 2014). They consist of upper crustal, doubly-vergent orogenic prism that developed from the inversion of a former Mesozoic basin and from basement stacking, and grew diachronously from east to west. The northern side of the belt, known as the North Pyrenean Zone (Fig. 1) is constituted by inverted extensional Mesozoic basins, that are flanked by the Aquitaine basin to the north (Lagabrielle et al., 2010, and references therein). The southern side (South Pyrenean Zone) is characterised by a basement-involved thrust stack that in the west-central Pyrenees is composed of three main

77 thrust sheets, flanked to the south by the Ebro basin: The Lakora-Eaux-Chaudes, Gavarnie and
78 Guarga thrust sheets (Teixell, 1996; Labaume et al., 2016) (Fig. 1B). These thrust sheets involve
79 Paleozoic basement and a cover assemblage with preorogenic Mesozoic rocks and a foreland
80 basin sequence of late Cretaceous to early Miocene rocks. These synorogenic rocks of late
81 Santonian to early Miocene age constitute the South Pyrenean foreland basin which, during
82 Eocene times, concentrated the fluvio-deltaic sedimentation in the Àger and Tremp Graus
83 basins, to the east, that funneled sediments to the west, to the slope and deep-marine Ainsa
84 and Jaca basins (Nijman and Nio, 1975; Puigdefàbregas et al., 1992; Caja et al., 2010).
85 The deep-marine sedimentation in the Jaca basin accumulated a thick turbiditic succession (Fig.
86 1B), known as the Hecho Group (Mutti, 1985). The Hecho Group (lower-middle Eocene) was
87 mainly fed axially from eastern source areas, located in the uplifting Pyrenees and the Ebro
88 Massif to the south (Caja et al., 2010; Gómez-Gras et al., 2016). The end of turbiditic
89 sedimentation is characterised by the occurrence of a turbiditic channel, known as the Rapitán
90 channel (Remacha et al., 1995), that already displays paleocurrents from the north and records
91 the first sediment input from new emerged source areas located immediately north of the basin.
92 From that time, turbidite sedimentation was replaced by shallow marine and transitional
93 environments (starting in the Bartonian; Oms et al., 2003) when the basin depocentre migrated
94 to the south, to the central part of the basin (Teixell, 1996). The first delta slope sediments are
95 the Larrés marls (Fig. 2), which are related to the delta front deposits of the Sabiñánigo
96 sandstone Formation (Puigdefàbregas, 1975). Overlying these deposits, the Pamplona Marls
97 (Mangin, 1960) (Figs. 2, 3) represent the delta slope sediments of the Belsué-Atarés Formation
98 (Priabonian). These delta sediments are followed by coastal and terrestrial deposits of the
99 Campodarbe Group (upper Eocene-lower Oligocene molasse) that represent the overfilled stage
100 of the basin and are the last unit preserved in the basin (Puigdefàbregas, 1975; Labaume et al.,
101 1985; Barnolas and Teixell, 1994; Oliva-Urcia et al., 2015). The transition from marine to
102 terrestrial environments in the basin is diachronic, following the main westward progradation

of sedimentary systems (Puigdefàbregas, 1975; Dreyer et al., 1999), that ends with generalised continental sediments marking the closure and the initiation of an endorheic basin stage, dated to 36 Ma (Ortí et al., 1986; Payros et al., 1999; Barnolas and Gil-Peña, 2002; Costa et al., 2010). The Campodarbe Group reaches a thickness of more than 3000 m in the central part of the basin (Guarga syncline, Fig. 1B), where two main sediment routings can be identified: an east-derived fluvial system that enters through the southeastern part of the basin, and a north-derived alluvial fan system that characterizes the northern part of the basin (Puigdefàbregas, 1975; Montes and Colombo, 1996). The order of formation of these north-derived alluvial fans is first the Santa Orosia (Priabonian according to Oms et al., 2003), Canciás, then the Peña Oroel, and finally the San Juan de la Peña fan (Figs. 2, 3) (Oligocene-Miocene according to Puigdefàbregas, 1975; early Oligocene according to Hogan and Burbank, 1996). Nonetheless, the lack of available data regarding the precise age span of each alluvial fans does not allow for accurate correlation. The transitional facies of the Belsué-Atarés Formation are mainly represented by mouth-bar deposits, with a general westward progradation throughout the basin, controlled by growing fold structures (Puigdefàbregas, 1975; Hogan, 1993; Labaume et al., 2016) (e.g., Yebra de Basa and Atarés anticlines, Fig. 2). The overlying fluvial deposits of the Campodarbe Group are mainly represented by the alternation of yellow shales with isolated sandstone channels in the lower part, that grade upwards to red coloured shales and paleosols, linked with the thick conglomeratic successions that are concentrated in synsedimentary synclines (Figs. 2, 3).

2.2 Source-rock lithologies

Potential source terranes for the Jaca basin during the late Eocene-Oligocene can be divided into: (i) the Paleozoic basement of the Axial Zone, (ii) the preorogenic Mesozoic cover successions, and (iii) a synorogenic assemblage of late Cretaceous-middle Eocene deposits. To the north, the Axial Zone (Fig. 4) forms the core of the Pyrenean belt. It is constituted by an

assemblage of Cambro-Ordovician to Devonian metasedimentary units, followed by Carboniferous flysch deposits, which are in turn intruded by Variscan granitoids (Carboniferous-Permian) (Debon et al., 1996). These rocks are unconformably overlain by Permo-Triassic red beds, or directly by Cretaceous limestones. The Mesozoic succession is constituted, when complete, of Triassic shales, carbonates, evaporites and dolerites (Muschelkalk and Keuper facies), followed by thick carbonate and sandstone-shale successions of Jurassic and Cretaceous age. In the North Pyrenean Zone (Fig. 4), the Jurassic-Cretaceous succession is represented by carbonates that are followed by a thick succession of deep water shales and turbidites of Aptian to late Cretaceous age, intruded by basaltic subvolcanic rocks (Azambre, 1967). In contrast, in the South Pyrenean Zone (Fig. 4), Cretaceous to lower Ypresian terranes are mainly represented by platform carbonates that constitute thick accumulations of limestone, dolostone and sandy deposits (e.g., the Marboré Sandstone; Souquet, 1967). The youngest set of potential source rocks are those that form the Eocene clastic infill of the Àger, Tremp, Ainsa and Jaca basins, which mainly consist of siliciclastic alluvial, deltaic and turbidite deposits (Figs. 1, 4).

3. SAMPLING AND METHODS

The four main fan areas (Santa Orosia, Canciás, Peña Oroel and San Juan de la Peña) were described by stratigraphic logs (Figs. 2, 3) that show the transition from the deltaic/fluvial to alluvial fan environments. In addition, two complementary sections (Sabiñánigo and Abenilla areas) were studied in order to obtain a better resolution in the correlations between the eastern sector (Canciás and Santa Orosia) and the western sector (Peña Oroel and San Juan de la Peña), which are also dissected by the Yebra de Basa anticline-Jaca thrust (Fig. 2). Data from the Santa Orosia section were published by Roigé et al. (2016) and here are further discussed and reinterpreted.

One hundred twelve sandstone and conglomerate samples were collected from the four alluvial fan areas. The number and spacing of samples were established according to the representativeness of each analysed sedimentary system along the stratigraphic logs. Seventy-two samples were chosen for quantification of the detrital modes through point counting analysis under the polarizing microscope. Thin sections were prepared and stained using Na-cobaltinitrite (Chayes, 1952) for suitable identification of feldspar, and Alizarine red-S staining for distinction of carbonate composition, such as dolomite, ankerite and calcite.

The proportions of each detrital modes were established using the Gazzi-Dickinson point counting method (Gazzi, 1966; Dickinson, 1970; Ingersoll et al., 1984; Zuffa, 1985). Three hundred to five hundred points were counted for each thin section (Dryden, 1931), and classified in 104 petrographic classes (including framework grains, diagenetic minerals, matrix and porosity). All the framework grains were labeled according to the main four classes established by Zuffa (1980): non carbonate extrabasinal (NCE), non carbonate intrabasinal (NCI), carbonate extrabasinal (CE), and carbonate intrabasinal (CI). Metamorphic rock fragments were classified according to their composition and metamorphic rank (Garzanti and Vezzoli, 2003). Classification of volcanic grains was performed following the criteria of Marsaglia (1992) and Critelli and Ingersoll (1995). As sandstone rock fragments are largely represented in most of the studied samples, and constitute an important criteria for provenance interpretations, they were classified according to their main compositional features. Those sandstone rock fragments containing both intrabasinal and extrabasinal carbonate grains, with certain siliciclastic content and general well-sorting, were labeled as “Hybrid sandstone fragments”. This label is used according arenite classification by Zuffa (1980), and coincides with the general sandstone classification applied to the Hecho Group turbidites by Fontana et al. (1989) and Caja et al. (2010). Following the guidelines by Zuffa (1985), samples were plotted and classified into first to fourth order ternary diagrams. Petrofacies were represented in ternary diagrams, and mean

179 confidence regions (90%) were calculated for each of these with the “CoDaPack” software
180 (Comas-Cufí and Thió-Henestrosa, 2011).
181 In addition to the analysis of sandstone and the sandy matrix of conglomerate beds, a number
182 of outcrops were selected for point counting of clast lithologies. There were two clast-counting
183 locations in the Canciás fan, four in the Santa Orosia fan, four in the Peña Oroel fan and four in
184 the San Juan de la Peña fan. Procedures for clast counting followed the method of Howard
185 (1993), consisting at counting four closely spaced subsets of 100 clasts each, obtaining a total of
186 400 clasts for each studied location. In cases where identification of the clast lithology was
187 difficult, their nature was determined in thin sections. Some of the potential source areas for
188 these alluvial fans in the hinterland of the Jaca basin were also sampled, mainly located in the
189 Axial Zone, the Internal Sierras and the North Pyrenean Zone (Fig. 4), and compared to clasts
190 and rock fragments contained in the alluvial fans.
191
192 4. RESULTS
193
194 Samples of the Jaca basin contain a wide variety of grain types, here described and classified in
195 the four classes referred above (NCE, CE, NCI and CI). All the studied samples are grain supported
196 with a very low matrix ratio (less than 5% in most of them) and moderately to well sorted.
197 Authigenic minerals are related to cementation processes in most of the cases where calcite is
198 the main cement typology.
199
200 4.1 Grain types
201 4.1.1 NCE
202
203 Non-carbonate extrabasinal grains are those originated in the source area which lack a dominant
204 carbonatic composition, such as quartz, feldspar or lithic fragments (Fig. 5A).

Quartz is a common component that appears in all samples, with proportions ranging from 1.5% to 45.5%. It has been classified as monocrystalline (undulose or non-undulose), polycrystalline (with 2-3 or >3 subgrains) or contained in a rock fragment (sandstone or plutonic rock). Quartz with evaporitic inclusions (anhydrite and halite) has also been classified as it occurs in a large number of samples in proportions over 1-2% (Fig. 5E).

Feldspar is also a common component (up to 6.5%). Three types of feldspars distinguished are orthoclase (<4%), microcline (<1.2%) and plagioclase (<1.9%). K-feldspar (Fig. 5A) appears non-altered or, occasionally, slightly altered, while plagioclase usually shows higher degrees of alteration.

Lithic grains are widely represented in all the samples, being in some cases the most dominant component. Grains included in this type are metamorphic, volcanic, non-carbonatic sedimentary and plutonic rock fragments. According to the criteria of Garzanti and Vezzoli (2003), metamorphic rock fragments (Fig. 5A) are: (i) very low to low-grade (metapelites and phyllites), (ii) medium-grade (mica schists, schists and chlorithic schists), and (iii) high-grade (meta-quartzite and micaceous quartzite).

Igneous grains are predominantly granitoid rock fragments (0.25% to 3%) and volcanic lithics. Following the classification of Marsaglia (1992) and Critelli and Ingersoll (1995), three textures of paleovolcanic lithics have been identified: (i) lathwork texture made of plagioclase and altered augite (Fig. 5C), (ii) microlithic texture made of plagioclase microlites and, in lower proportions, (iii) vitric texture. Muscovite, biotite, chlorititzed biotite and chlorite are the most common phyllosilicate grains (<1%), appearing often as rock forming fragments, in schists or granitoids.

Non-carbonate sedimentary rock fragments are widely represented in most samples. Within this category, distinction is made between sandstone (Fig. 5B), hybrid sandstone (Fig. 5D), siltstone, hybrid siltstone and silicified rock fragments. Silicified rock fragments have been also subdivided into radiolarite rock fragments (Fig. 5D) and silicified limestones (Fig. 5F). Heavy minerals are always less than 1.5%, and are mainly zircon, tourmaline, apatite, titanite and epidote.

231

232 4.1.2 NCI

233

234 Non-carbonate intrabasinal grains are not a common component, and they appear always in
235 minor proportions as glauconite and argillaceous rip-up clasts. Glauconite is scarce, reaching
236 proportions close to 1% in some samples.

237

238 4.1.3 CE

239

240 Carbonate extrabasinal grains appear in all samples with a variety of textures (Fig. 6), being in
241 some cases the most dominant component (up to 78% of the total framework grains). A high
242 number of carbonate fragment typologies have been identified, such as (i) bioclastic and sparitic
243 limestones, (ii) dolostones, and (iii) dolomitic and dolomitized limestones. Fragments of
244 bioclastic limestones (Fig. 6A) were classified according Dunham (1962), appearing as micritic
245 and bioclastic mudstone (<22%), packestone-wackestone (<27%), and grainstone (<15%) (Fig.
246 6B, C). Sparitic limestone fragments are also present, and appear as monocrystalline calcite or
247 as polycrystalline sparitic calcite fragments (Fig. 6F).
248 Dolostone fragments (Fig. 6F) have been recognized as dolomicrite (<1%), polycrystalline sparitic
249 fragments (<7%) and single-grain dolomite.
250 Some of the alluvial fan samples of late Priabonian-Oligocene age exhibit significant amounts of
251 marine bioclasts (Fig. 6C-6E) as foraminifera (nummulitids, discocyclinids, miliolids), red algae or
252 bivalves. This marine faunal content is not consistent with the terrestrial environments
253 interpreted for the alluvial fans, so marine bioclasts have been classified as carbonatic
254 extrabasinal grains.

255

256 4.1.4 CI

Carbonate intrabasinal grains are mainly marine bioclasts (<15%), and subordinate micritic intraclasts and caliche concretions (<1%). Bioclasts have been grouped in (i) larger benthic foraminifera and planktonic foraminifera (nummulitids, discocyclinids and milliolids), (ii) other bioclasts, red and green algae, bivalves, ostracods, bryozoans and corals, and (iii) silicified bioclasts and calcite cement replacing bioclasts.

4.2 Clast types

The most common clast type are hybrid sandstone clasts, which have been classified according to granulometry (very fine, fine, medium, coarse, and very coarse grained). Some of these clasts show internal gradation or lamination, and are distinctive among other sandstone clasts for their yellowish-brown colour.

Quartzarenite and/or siliciclastic sandstone or siltstone (occasionally red-coloured) clasts appear in minor proportions. A few conglomerate and metamorphic-rich breccia clasts have been also found in almost all the alluvial fans.

Limestone clasts are also represented in all the alluvial fans. Grey limestones with a fossiliferous content are the most abundant clasts, together with grey limestones with bedded black chert. Grainstone and packstone clasts also occur, with bioclasts like alveolines, nummulites, orbitolines, bivalves, rudists or red algae. Other kind of limestone like white calcareous mudstones or boundstone clasts have been also identified. Black and orange calcarenites are subordinate, together with some carbonatic breccia clasts. Dolostone clasts are dark-grey with a sucrosic texture.

Plutonic rock clasts are represented by granitoids, that have been observed either altered or fresh, in some cases affected by albitization (pink granitic clasts). Green subvolcanic clasts are a distinctive component in most of the alluvial fans, while volcanic clasts are scarce but easy to

distinguish due to their vesicular texture. Metamorphic rock clasts are mainly quartzites (commonly green-coloured), and some scattered hornfelsic schists and tourmaline-bearing schists.

4.3 Petrofacies

The analysis of the deltaic and alluvial sandy systems identifies four main petrofacies, according to characteristic and significant compositional variations. The assignment of each petrofacies takes into account vertical and lateral compositional variations, and highlights the relevance of extrabasinal grains which provide valuable information on source areas.

4.3.1 Hybrid clast-dominated petrofacies

The main feature of this petrofacies (Fig. 7A) is the high content of hybrid sandstone/siltstone rock fragments (>10%). Hybrid rock fragments are considered to be those that contain both extrabasinal and intrabasinal carbonate components, in similar proportions. Hybrid sandstone rock fragments are usually accompanied by limestone rock fragments, which are commonly the second most important component in this petrofacies, and by significant amounts of marine bioclasts. This petrofacies is also characterised by a low content of siliciclastic components (metamorphic and sandstone rock fragments).

4.3.2 Carbonate extrabasinal enriched petrofacies

Carbonate grains are the most dominant rock fragment (Fig. 7B) in this petrofacies (>45%). Mudstone and wackestone rock fragments widely occur among the carbonatic grains, while grainstone, packstone and dolostone rock fragments are also widespread. Hybrid sandstone

rock fragments can also occur, but are subordinate (<15%) to the carbonate ones. As in the "Hybrid clast-dominated" petrofacies, the siliciclastic content is very low. Intrabasinal grains are mainly reworked caliche nodules.

4.3.3 Siliciclastic dominant petrofacies

This petrofacies is not well represented although distinctive in the study area. Siliciclastic components are the most dominant grain type (Fig. 7C), always with less than 30% of carbonatic grains and less than 5% of hybrid sandstone rock fragments. Shales, schists and quartzites are always present in this petrofacies, together with significant amounts of quartz grains, as well as radiolarite rock fragments and quartz-rich sandstone rock fragments. Other subordinate sandstone/siltstone rock fragments that usually appear are those with mica and opaques. Feldspars occur as orthoclase, microcline and plagioclase, with a Plagioclase/K-feldspar ratio of <1.

4.3.4 Mixed lithic and carbonate petrofacies

The "Mixed lithic and carbonatic" petrofacies is characterised by 15-40% carbonate grains (Fig. 7D), hybrid sandstone rock fragments (up to 30 %) and higher proportions of lithic grains (25-35%, excluding hybrid sandstone fragments) when compared with the "Hybrid clast-dominated" and "Carbonatic extrabasinal enriched" petrofacies. Non carbonatic grains are mainly represented by quartz, K-feldspar, shales and schists and occasional radiolarite rock fragments. Most of the carbonatic grains are extrabasinal, but intrabasinal grains can also be found in this petrofacies.

4.4 Modal sandstone composition and clast point counting

335

336 Sandstone detrital modes of the analysed systems have been plotted using ternary diagrams, in
337 order to classify and illustrate compositional trends and potential shifts in the source areas. A
338 first-order compositional classification (Figs. 8A, 9A, 10A, 11A) has been applied according to
339 Zuffa (1980), which represents the relative content on "Non-carbonate extrabasinal" (NCE),
340 "Carbonate extrabasinal" (CE) and "Carbonate intrabasinal" (CI) components, and distinguishes
341 between litharenites, calclithites and hybrid arenites. The Quartz-Feldspar-Lithics (Q-F-L)
342 diagram is used as second-order classification ternary diagram (Figs. 8B, 9B, 10B, 11B) (according
343 to Dickinson et al., 1983), while Lithic metamorphic-Lithic volcanic-Lithic sedimentary (Lm-Lv-Ls)
344 is used as third-order ternary diagram (Fig. 12A). A fourth-order ternary diagram discriminates
345 among the described petrofacies comparing hybrid sandstone fragments (Hybrid Snd), feldspar
346 and lithic fragments, excluding hybrid sandstone fragments (F+L) and CE (Figs. 12B, 13). Using
347 these ternary diagrams, we present a description of each of the analysed stratigraphic sections,
348 ordered according to the relative age of the alluvial fans.
349

350 4.4.1 Santa Orosia section
351

352 This section (Figs. 3, 8) starts with the deltaic sandstones of the Belsué-Atarés Formation
353 (samples JY19 to JY22; Fig. 8), which are constituted by 550 m-thick, thickening and coarsening-
354 up cycles, interpreted as mouth-bar deposits (Puigdefàbregas, 1975) alternated with marls,
355 occasionally with abundant bioclastic content. These delta sandstones are characterised by a
356 similar proportion of CE and NCE grains, with some presence of bioclastic content in the
357 trangressive facies, giving a mean composition of $NCE_{48}CE_{50}CI_2$. According to these proportions,
358 samples of the Belsué-Atarés Formation can be classified as calclithites (Fig. 8A) in the sense of
359 Zuffa (1980). In terms of siliciclastic components, the mean composition is $Q_{70}F_6L_{24}$. CE grains
360 mainly consist of biomicritic mudstone fragments and detrital dolomite grains (Roigé et al.,

2016). The lithic population is represented by metamorphic rock fragments as phyllites as well as siliciclastic sandstone and siltstone rock fragments. Due to the high content of CE, samples of the Belsué-Atarés Formation belong to the "Carbonate extrabasinal enriched" petrofacies.

Overlying these delta deposits there is a succession of channelised conglomerates (490 m thick) alternated with yellow-to-grey claystones represent the Santa Orosia fan (samples JY23 to JY35, JY38 and JY39; Fig. 8). This fan records a major change in the type of petrofacies due to appearance of hybrid sandstone fragments. These fragments increase up to 40% towards the top of the unit. The second most common component are limestone rock fragments (30-50%), whilst plutonic, subvolcanic and sandstone rock fragments are subordinate. The clast population of conglomerate beds is also dominated by hybrid sandstone clasts (40-80%) that increase in proportion upwards, thus displaying a similar trend as recorded in sandy fraction (Fig. 8C-F). Limestone clasts (10-30%) decrease upwards and appear mainly as fossiliferous grey limestones (Fig. 8H-I) or as silicified limestones with bedded chert. Some scattered pebbles of metamorphic-rich breccias, green dolerites (ophites) (Fig. 8G) and granitic clasts have also been found. Most of the samples are litharenites, with a mean of $NCE_{52}CE_{46}CI_2$ and $Q_{33}F_7L_{60}$ (Fig. 8A, B). According to these compositional features, all the samples can be assigned to "Hybrid clast-dominated" petrofacies.

The uppermost conglomerate beds of this section belong to the Canciás alluvial fan (samples JY36 and JY37; Fig. 8), which records a significant decrease in the hybrid sandstone rock fragments and an increase of the carbonatic extrabasinal components (Roigé et al., 2016). Both sandstone and pebble counts display this trend, being clearer in the sandy fraction, where CE grains reach 55 to 70% (Fig. 8A-F). Therefore the "Carbonatic extrabasinal enriched" petrofacies dominate this upper part of the section.

4.4.2 – Canciás section

387 The Canciás section (Figs. 3, 9) also starts with the transitional deposits of the Belsué-Atarés
388 Formation (850 m thick), which are represented by an alternation of sandy mouth-bar deposits
389 and bioclastic marls (samples CANC1 to CANC5; Fig. 9). Most of the samples present a
390 predominance of carbonate extrabasinal grains (Fig. 9A) that allow them to be classified as
391 calclithites (mean of $NCE_{44}CE_{54}CI_2$ and $Q_{30}F_3L_{67}$). Carbonate extrabasinal grains are mudstone,
392 bioclastic grainstone/packstone limestone fragments and minor proportions of dolostone rock
393 fragments, while intrabasinal carbonatic components are very low. Lithic grains consist on
394 sandstone (up to 5%), hybrid sandstone (5-12%) and low-grade metamorphic rock fragments
395 (<4%). This association of grains allows definition of a "Carbonate extrabasinal enriched"
396 petrofacies (CANC1, CANC3 to CANC5). Nonetheless a distinctive petrographic signature is also
397 recorded in one sample (CANC2), that is characterized by an increase of non-carbonate
398 extrabasinal grains (up to 70%), with single quartz grains, feldspars (orthoclase, plagioclase and
399 microcline) and lithic grains (up to 30%). Metamorphic grains (shales and schists) are more
400 common than sandstone/siltstone fragments, and hybrid sandstone grains are very low (<2.5%).
401 According to these components and proportions, sample CANC2 can be included in the
402 "Siliciclastic dominant" petrofacies.
403 These transitional deposits change progressively upwards to alluvial-fluvial deposits (1800 m
404 thick) constituted by channelized sandstone bodies passing laterally to red-coloured paleosoils.
405 The succession terminates with thick massive conglomerates (up to 50 m) of the Canciás fan
406 (samples CANC 6-19; Fig. 9). These alluvial deposits are quite similar to those of the Santa Orosia
407 fan, where hybrid sandstone and siltstone rock fragments increase upwards (Fig. 9A, B) reaching
408 45% of the total framework grains (means of $NCE_{48}CE_{51}CI_1$ and $Q_{33}F_1L_{66}$). However, this trend is
409 halted in the upper part of the section, where limestone fragments represent up to 78% of the
410 framework grains, while hybrid sandstone fragments gradually decrease. Limestone fragments
411 include bioclastic limestones (nummulites, alveolines, phytonellids), mudstone and dolostone
412 fragments. Metamorphic grains also occur along the section, with schist fragments that are the

most common non-sedimentary grain type, followed by plutonic and subvolcanic rock fragments. According to the results, the mid-lower part of the Canciás fan shows "Hybrid clasts dominant" petrofacies (CANC6 to CANC17), that evolves upwards to "Carbonate extrabasinal rich" petrofacies (CANC18 and CANC19). Clast populations also display this trend (Fig. 9C, D), reaching up to 60% of limestone pebbles, which are dominantly grey mudstone (sometimes with nodular and some scarce bedded chert) and fossiliferous limestones (e.g., packstone with orbitolina). Unaltered granitic pebbles also occur (Fig. 9E), together with limestone-breccias (Fig. 9F, G), volcanic pebbles and quartzite pebbles.

4.4.3 Abenilla-Sabiñánigo area

The Abenilla and Sabiñánigo area (Fig. 2) was sampled to help trace the compositional associations of the Santa Orosia, Canciás and Peña Oroel sections.

The transitional deposits of the Belsué-Atarés Formation in the Abenilla section (Fig. 2) exhibit a dominance of hybrid sandstone and siltstone rock fragments. The overlying conglomeratic facies show a composition similar to the older deltaic deposits, dominated by high amounts of hybrid sandstone rock fragments (up to 30%). Bioclastic limestones are the most represented among the carbonatic grains, while some silicified limestones also occur. Feldspar content is low (1%) and lithic fragments like metamorphic (schists and shales) and volcanic rock fragments reach 2% and 3% respectively. Means for this section are $NCE_{52}CE_{48}Cl_0$ and $Q_{25}F_1L_{74}$.

Further west, in the Sabiñánigo section, the Belsué-Atarés Formation (Fig. 2) shows an increase in hybrid sandstone rock fragments from base to top, while siliciclastic sandstone and siltstone grains decrease. The conglomeratic beds (Campodarbe Group) that lie above these deltaic deposits show increased hybrid sandstone grains to a maximum of around 35%. Limestone fragments are very similar to those found in the Abenilla section, with silicified limestone fragments also represented in all the samples. Some of the alluvial fan conglomerates show

439 significant amounts of marine bioclasts (up to 10%) like nummulites, bryozoa, red algae and
440 bivalves. With regard to the clast population, hybrid sandstone clasts dominate (63%) while grey
441 limestones are the second most represented lithology (32%). Limestone with bedded chert
442 clasts appear also widespread, while black dolostone and green subvolcanic clasts are scarce
443 (<1%). Mean values are $NCE_{58}CE_{39}Cl_3$ and $Q_{26}F_2L_{72}$. According to these compositional features, all
444 the samples can be included in the "Hybrid clast-dominated" petrofacies.
445
446 4.4.4 Peña Oroel section
447
448 As in the Santa Orosia and Canciás sections, the Peña Oroel section (Figs. 3, 10) starts with the
449 deltaic deposits of the Belsué-Atarés Formation (samples JJ1 to JJ8; Fig. 10). The lower part of
450 this section is dominated by 800 m-thick mouth-bar sandstones punctuated by coral buildups
451 (1.5 m thick), which change upwards to 110 m-thick channelized sandstones and red bioturbated
452 siltstones, interpreted as delta plain deposits (Puigdefàbregas, 1975). Most samples of this
453 formation show a predominance of the non-carbonatic extrabasinal grains (Fig. 10A) over the
454 carbonatic extrabasinal grains (mean values are $NCE_{61}CE_{28}Cl_{11}$ and $Q_{44}F_3L_{53}$). Intrabasinal
455 carbonate grains are quite common, reaching up to 17% of the total framework grains, where
456 foraminifera (nummulitids and miliolids), red algae and bivalves are the most represented
457 bioclast type. Carbonatic extrabasinal grains (13-40%) are mainly mudstone and bioclastic
458 limestone fragments. Silicified rock fragments, most likely silicified limestones, are quite
459 abundant, reaching close to 8%. Quartz monocrystalline grains are dominant over
460 polycrystalline, and show an increasing upwards trend. Other siliciclastic grains like feldspars
461 (Plagioclase/K-feldspar <1) and metamorphic fragments appear in low percentages, mainly in
462 the lower part of the section (Fig. 10B). Hybrid sandstone/siltstone rock fragments (up to 38%)
463 decrease towards the upper part, reaching close to 10%. This decreasing trend can also be
464 observed in the proportion of limestone fragments, while siliciclastic grains, as quartz and

metamorphic fragments, increase to the top of the formation (up to 60%). According to these results, the lower part can be assigned to “Hybrid clast-dominated” petrofacies (JJ1, JJ3, JJ5, JJ7B, JJ7S), while in the upper part some samples can be classified as “Mixed lithic and carbonatic” petrofacies (samples JJ6 and JJ8).

Overlying the Belsué-Atarés Formation, alluvial fan deposits constitute the thickest part of the section (1300 m) formed by massive and structureless conglomeratic beds alternating with highly bioturbated sandstone bodies (samples JJ9 to JJ25; Fig. 10). Sandstone composition displays a change by a decrease in the non-sedimentary lithic fragments and quartz grains, and an increase of the hybrid sandstone rock fragments (up to 70%) until the top of the Peña Oroel fan (means of $NCE_{74}CE_{23}Cl_3$ and $Q_{16}F_1L_{83}$). Carbonate extrabasinal grains are limestone fragments (10-40%), and some marine bioclastic grains (foraminifera, algae, bivalves). Conglomeratic beds show a very monotonous clast composition (Fig. 10C-G) made up by dominant hybrid sandstone clasts (80-90%), limestone and silicified limestone clasts (mainly with bedded chert, Fig. 10H) and some scattered white quartz pebbles. Highlighting the absence of any plutonic or metamorphic clasts, the only type of non-sedimentary lithology that has been found in the conglomeratic beds is a characteristic volcanic clast with amygdaloidal texture (Fig. 10I). This composition assemblage corresponds to the “Hybrid clast-dominated” petrofacies (JJ9 to JJ25) which dominates along all the Peña Oroel alluvial fan, being the system with the highest content of hybrid sandstone rock fragments.

4.4.5 San Juan de la Peña section

The first samples of the San Juan de la Peña section (Figs. 3, 11) belong to the Campodarbe Group (samples SP17, SP21 and SP9), which is represented by a relatively thick (1150 m) succession of fluvial deposits formed by the alternation of yellow siltstones and isolated sandstone channels. Non carbonate extrabasinal grains (70-90%) dominate over the carbonate

491 extrabasinal ones (<30%), and intrabasinal components are lacking (means of $NCE_{80}CE_{20}Cl_0$ and
492 $Q_{47}F_2L_{51}$) (Fig. 11A, B). Mono- and polycrystalline quartz grains reach proportions of 25%, while
493 feldspars are low represented (<3%), with a Plagioclase/K-feldspar ratio of <1. Among the lithic
494 grains, metamorphic rock fragments prevail (up to 20%) and appear as phyllites, schists and
495 quarzites, while siliciclastic sandstone fragments are the second most represented lithic grains.
496 Some characteristic lithic fragments of sandstone and siltstone rock fragments with
497 ferrouginous cements also appear, together with lower amounts of radiolarite, subvolcanic
498 dolerites and silicified rock fragments. Carbonate extrabasinal grains are mainly mudstone rock
499 fragments while grainstone and other bioclastic rich fragments are scarce. According to these
500 compositional features, samples can be classified as “Siliciclastic dominant” petrofacies.
501 Close to the ocurrence of the first conglomeratic beds related to the San Juan de la Peña fan
502 (sample SP1 in Fig. 11), some fluvial deposits of the Campodarbe Group already show a
503 compositional change (sample SP20). This change is evidenced by the appearance of large
504 amounts of sandstone/siltstone hybrid rock fragments and by a decrease of the quartz and
505 metamorphic grains (Fig. 11A, B). Mean values are $NCE_{51}CE_{47}Cl_2$ and $Q_{24}F_1L_{75}$. A characteristic
506 feature of all the fluvial-alluvial sediments of the San Juan de la Peña fan is the significant
507 amounts of marine bioclastic grains (up to 6%) such as resedimented benthic foraminifera, red
508 algae, bivalves or bryozoans (Fig. 6E). The San Juan de la Peña fan is characterised by an
509 alternation of 1250 m-thick sandstone and conglomerate beds grading into massive (90 m),
510 structureless conglomerates. These alluvial deposits display an increasing trend of the hybrid
511 sandstone fragments towards the top of the unit that can be also identified in the pebble
512 fraction of the conglomeratic beds (Fig. 11C-F). However, the upper part of the section (SP14,
513 SP15) show a slight increase of lithic components when compared to the Peña Oroel fan. Clast
514 composition is ruled by the mentioned hybrid sandstone clasts (increasing upwards from 65%
515 to 85%) and limestone clasts (some of them silicified, with bedded chert), but some other
516 lithologies have been identified, such as clasts of granites, hornfelsic schists, green subvolcanic

517 dolerites, quartzites and some conglomerate and metamorphic-rich breccia clasts (<1%) (Fig.
518 11G-I). As evidenced by the large amounts of hybrid sandstone fragments, the San Juan de la
519 Peña fan samples can be assigned to the "Hybrid clast-dominated" petrofacies (samples SP1-
520 SP8), although the slightly increase in lithic components recorded in the uppermost part of the
521 section means that samples SP15 and SP14 (Fig. 11) can be attributed to the "Mixed lithic and
522 carbonatic" petrofacies.
523
524 4.4.6 Sandstone composition trends
525
526 According to the results presented above, similar compositional trends are identified in each of
527 the analysed sections. In order to compare the evolution of detrital modes from deltaic to
528 alluvial environments, third order (Lm-Lv-Ls) to fourth order (H.Snd-F+L-CE) ternary diagrams
529 were created (Fig. 12). For lithic grains (Lm-Lv-Ls), deltaic deposits from the Santa Orosia and
530 Canciás sections, together with the lower fluvial deposits of San Juan de la Peña section, show
531 high concentrations of lithic metamorphic grains. In constrast, all the alluvial fans are ruled by
532 lithic sedimentary grains (Fig. 12A). This trend can also be identified in the fourth order diagrams
533 (H.Snd-F+L-CE). In each of the analysed sections, the higher concentrations of hybrid sandstone
534 fragments are recorded in the alluvial conglomerates, while deltaic and fluvial deposits are
535 richer in extrabasinal carbonates and/or siliciclastic rock fragments (metamorphics and
536 feldspars) (Fig. 12B).
537
538 5. DISCUSSION
539
540 To unravel the provenance of the sedimentary systems that constitue the infill of the South
541 Pyrenean basin is a challenging task due to the few distinctive rocks to constrain a restricted
542 source area. For this reason, the association of grain provenance with petrofacies is here used

to elucidate the nature and location of the most likely source areas and relate these to the tectonic evolution of the west-central Pyrenean thrust belt.

5.1 Detrital provenance: identification of source rock types

5.1.1 Provenance of sand grain types

Siliciclastic grains such quartz or feldspar can be sourced from a wide variety of rocks as they are contained in many rocks of the Paleozoic basement (Axial Zone), and also in the Mesozoic and Tertiary detrital rocks of the southern Pyrenees. Nonetheless a few characteristic features can help recognising the provenance of these grains. Well-rounded quartz is usually atributted to recycling of previous sandy systems (i.e., Fontana et al., 1989) or to long distance transport and intense weathering conditions. Few of these grains show inherited quartz overgrowths that could be associated with recycling of Paleozoic (Carboniferous or Permian formations), Cretaceous formations (Marboré Sandstone) or Eocene sandstones (Pardina Formation). Quartz with evaporitic inclusions (halite and anhydrite) are widespread in most of the analyzed samples and can be linked to erosion of the Triassic Keuper evaporite facies (Marfil, 1970).

Feldspar grains like orthoclase, microcline or plagioclase are attributed to granitoid and metamorphic rock sources from the Paleozoic basement and also from Triassic dolerites (ophites). Erosion of the Paleozoic basement can be identified by the occurrence of metamorphic rock fragments, like schists, shales and quartzites, and plutonic fragments like granitoids. Other lithic grains like quartzarenite fragments can be linked to erosion of Carboniferous formations or the Permo-Triassic red beds, which are abundant in the Axial Zone. Subvolcanic rock fragments can be associated to the contribution of Triassic dolerites that crop out in the southern Pyrenees and also in the North Pyrenean Zone (i.e., Bedous unit and Chaînons Béarnais; Fig. 1B). Basic volcanic rock fragments could also be sourced from the Permian volcanic basins of the Axial Zone or from the basaltic rocks that crop out within the

569 Cenomanian-Turonian flysch of the North Pyrenean Zone. Hybrid sandstone/siltstone rock
570 fragments are attributed to recycling of the Eocene flysch basin (Hecho Group) and of deltaic
571 sediments of the South Pyrenean basin. Those grains dominate in most of the analysed samples,
572 and evidence the high degree of recycling of the turbidites from the former foreland basin of
573 the Pyrenees. The low quartz content in the Jaca basin is a compositional feature that evidences
574 the fact that recycling does not imply an enrichment in mechanically and chemically stable grains
575 (Zuffa, 1987; Di Giulio et al., 2003; Garzanti et al., 2013).
576 Terrigenous carbonate grains point to significant contributions from Mesozoic-Tertiary
577 carbonate sources, without evident supply from Paleozoic carbonates (e.g., Devonian
578 limestones). Carbonate fragments containing nummulitids or alveolinids are attributed to
579 erosion of the Paleocene-Eocene platform carbonates or carbonate megaturbidites, and those
580 containing *phitonellid* tests are linked to contributions from Turonian limestones (southern
581 Pyrenees). Dolostone or dolomitized fragments are interpreted as supplied from the Paleocene
582 formations presumably, while dolostones with sucrosic texture can be easily linked with erosion
583 of the Jurassic dolostones cropping out in the southern Pyrenees or in the North-Pyrenean Zone.
584 Bioclastic grains such as nummulitids, miliolids, bivalves and red algae that occur in samples
585 from terrestrial deposits, appear as single grains and with a high degree of preservation. These
586 features suggest Eocene marls of the deltaic formations or turbidite formations as the most
587 likely source areas for these bioclastic grains.
588
589 5.1.2 Provenance of clasts in conglomerates
590
591 Coupling sand with clast provenance allows for a more accurate correlation with the potential
592 sources for the alluvial fans. Compositional trends identified in the sandy fraction are very similar
593 to those identified in the clast population. In all the sections, the variation of the most
594 represented grain lithologies (i.e., hybrid sandstone and limestone) are displayed uniformly in

595 both sand and clast populations (Figs. 8-11). Large amounts of hybrid sandstone clasts are
596 identified in all the conglomeratic bodies, and can be attributed to erosion of the Hecho Group,
597 presently exposed in the northern part of the Jaca basin (Roigé et al., 2016).
598 As for the sandy fraction, limestone clasts containing bioclasts like numulitids or alveolinids are
599 interpreted as derived from the Paleocene-Eocene formations, present in the southern
600 Pyrenees. The interbedded megaturbidite beds within the Hecho Group that include large
601 limestone clasts of various sizes (Soler and Puigdefàbregas, 1970; Rupke, 1976; Labaume et al.,
602 1987) may represent an additional carbonate source for the alluvial fans. Limestone clasts with
603 chert nodules could derive from the Eocene time equivalents of the Alveolina Limestone in the
604 southern Axial Zone, or also from the Santonian Limestones that are part of the cover materials
605 of the Axial Zone in the west-central Pyrenees. A distinctive variety of clasts is the
606 limestone/calcarenite clasts with dark bedded chert (Figs. 10H, 11H) that are widely found in all
607 the alluvial fans. As mentioned above, there are many limestone formations that contain chert
608 nodules in the southern Pyrenees, but bedded chert is never reported. The formation that could
609 provide these kind of clasts may be the Coniacian flysch of the North Pyrenean Zone (Casteras
610 et al., 1970), which is described as a calcareous flysch with black bedded chert. In addition, the
611 planktonic foraminifera observed in some of these clasts suggest a Cenomanian-Turonian age.
612 Black dolostone also provide a distinctive type of clast due to its dark colour and poor
613 cementation. This kind of facies is characteristic of the Jurassic of the North Pyrenean Zone (e.g.,
614 Chaînons Béarnais; Fig. 1).
615 With regard to siliciclastic clasts, sandstone pebbles could be sourced from Mesozoic (mostly
616 Marboré Sandstone) or Paleozoic (Carboniferous or Permian sandstones) formations.
617 Characteristic green quartzite clasts could be attributed to erosion of the quartzites of the
618 “Green Formation” (Lith, 1965) reported in the Paleozoic basement of the entire Axial Zone.
619 Metamorphic clast-rich breccia pebbles are very similar to the well-known Ibarrondoa breccia
620 (late Cretaceous), a formation that crops out in the hanging-wall of the Lakora thrust (Teixell,

621 1996, and references therein) (Fig. 1), and is, therefore, indicative also of supply from the North
622 Pyrenean Zone.
623 Granitic clasts and metamorphics like schists and hornfelsic schists indicate supply from the
624 Paleozoic basement. Green subvolcanic ophite clasts are indicative of erosion of the Triassic
625 dolerites than could be derived either from the North Pyrenean Zone or the southern Pyrenees.
626 Volcanic clasts with amygdaloid texture can be linked with the alcaline volcanic rocks (late Albian
627 to Turonian) of the North Pyrenean Zone that consist mainly on teschenites and picrites
628 (Azambre, 1967).
629
630 5.2 Petrofacies distribution and provenance of the study formations
631
632 According to the grain provenance presented above, here we discuss the provenance of each
633 sedimentary units. In the Santa Orosia section, the Belsué-Atarés delta is represented by
634 “Carbonatic enriched” petrofacies (Fig. 13). The absence of significant amounts of hybrid
635 sandstone fragments, and the abundance of detrital dolomite grains together with paleocurrent
636 directions (Remacha and Picart, 1991) indicate supply from eastern source areas (Roigé et al.,
637 2016). The proximal time equivalent system of these deltaic sediments could be the lower part
638 of the fluvial Escanilla Formation of the Ainsa basin, according to its Priabonian age and its
639 dominant carbonate composition (Mochales et al., 2012; Michael, 2013). In contrast, the
640 overlying Santa Orosia fan has a northern provenance, according to paleocurrents and facies
641 architecture (Puigdefàbregas, 1975). From a petrologic point of view, this shift in source area is
642 evidenced by an increased amount of hybrid sandstone rock fragments, which derive from
643 erosion of the Hecho Group turbidites that were on top of the uplifting Axial Zone at this time
644 (Labaume et al., 2016; Roigé et al., 2016). This new source area implied a major paleogeographic
645 reorganization during Priabonian times related to the development of the basement-involved
646 Gavarnie thrust, whose activity has been set to the late Eocene-early Oligocene (Teixell, 1996;

Jolivet et al., 2007; Labaume et al., 2016). In contrast, the lateral equivalents of the Canciás alluvial fan, located in the top of the section, record a decrease of recycling from the turbiditic basin and an increase in carbonatic components that are related to erosion from the Paleocene/Eocene and Mesozoic formations (see below).

In the Canciás section, the transitional deposits of the Belsué-Atarés Formation are mainly represented by "Carbonatic extrabasinal enriched" petrofacies (Fig. 13) with some hybrid sandstone rock fragments, that are interpreted as eastern supply with initial contributions from the erosion of the turbiditic basin to the north (Gavarnie thrust zone). This eastern signal is replaced upwards by the predominant "Hybrid clast-dominated" petrofacies, widely represented in the bulk of the conglomerate beds of the Canciás fan (Fig. 13). The content of hybrid sandstone fragments from the Hecho Group increases upwards until the upper massive conglomeratic unit that shows a sharp change, evidenced by the high increase of Paleogene and Mesozoic limestone grains. This abrupt shift is intepreted as the erosion of source areas that were uncovered or slightly covered by the Hecho Group turbidites, that could be located in the the Peña Montañesa or Cotiella thrusts, to the north of the Ainsa basin.

The Abenilla and Sabiñánigo sections (Fig. 13), located between the Santa Orosia and Peña Oroel sections, are entirely represented by the "Hybrid clast-dominated" petrofacies and can be correlated to be the distal equivalents of the Santa Orosia and Canciás alluvial fans. The lack of an eastern source signal in the Belsué-Atarés delta in the Abenilla and Sabiñánigo areas indicates that there was no connection between these deltaic deposits and the deltaic ones from the Santa Orosia and Canciás sections at this time. We propose that, in this part of the basin, the delta sediments were fed by the prograding Santa Orosia fan, which evolved to the west to transitional shallow marine deposits (Figs. 3, 12), probably controlled by the growth of the Yebra de Basa anticline (Puigdefàbregas, 1975; Oms and Remacha, 1992; Labaume et al., 2016).

In the Peña Oroel section, the lower part of the Belsué-Atarés Formation shows a similar composition to the deltaic deposits of the Abenilla and Sabiñánigo areas, which consists of the

673 “Hybrid clast-dominated” petrofacies. Thus, here we also point to the Santa Orosia fan as the
674 proximal feeding system for these deltaic deposits. Nonetheless, the upper part of the Belsué-
675 Atarés Formation shows an increase on the siliciclastic components (feldspars and lithics), thus
676 being classified as “Mixed lithic and carbonatic” petrofacies (Figs. 12, 13). The coexistence of
677 significant amounts of grains sourced from the north (Hecho Group turbidites) and siliciclastic
678 components that could be derived from eastern source areas, indicate mixing of these two
679 different sediment routing systems. Once the deltaic sedimentation is replaced by the first
680 alluvial conglomeratic levels, the “Hybrid clast-dominated” petrofacies prevails throughout the
681 section, which implies a persistent and increased contribution from the Hecho Group turbidites.
682 In the San Juan de la Peña section (Fig. 13), the thick fluvial succession of the Campodarbe Group
683 displays “Siliciclastic dominant” petrofacies, with general paleocurrent directions to the west
684 and northwest (Puigdefàbregas, 1975). Thus, the source area of these fluvial sediments could
685 not be placed in the north, as seen in the Santa Orosia, Canciás and Peña Oroel fans, but must
686 be located to the east, in the the south-central Pyrenees, and funneled through the fluvial-
687 alluvial systems of the Ainsa basin (i.e., upper Escanilla Formation). These east-derived fluvial
688 sediments are replaced by the conglomerates of the San Juan de la Peña fan, which represent a
689 provenance shift, where the northern source area prevails, as evidenced by the presence of
690 “Hybrid clast-dominated” petrofacies.
691
692 5.3 Regional implications
693
694 In the Jaca basin, the first record of sediment with north-derived paleocurrents is found in the
695 last turbiditic channel of the Hecho Group, known as the Rapitán system (uppermost Lutetian;
696 Remacha et al., 1995; Roigé et al., 2016). Since then, the later deltaic systems (Sabiñánigo and
697 Belsué-Atarés Formations) show an interplay between the eastern and the northern sources
698 until the establishment of full terrestrial environments (Campodarbe Group, late Eocene-early

699 Oligocene), with predominant northern sources. Nonetheless, the fluvial facies of the lower
700 Campodarbe Group (late Eocene-early Oligocene) in the San Juan de la Peña section evidences
701 that sediment derived from eastern source areas still entered the basin when it became
702 internally drained (Puigdefàbregas, 1975), and while the Santa Orosia and Canciás alluvial fans
703 were already active. Thus, the switch between east-derived and north-derived sediment evolved
704 from east to west progressively through time, consistent with progradation of the systems and
705 with the diachronous uplift and exhumation of the Pyrenees from east to west (Fitzgerald et al.,
706 1999; Jolivet et al., 2007; Metcalf et al., 2009; Bosch et al., 2016; Labaume et al., 2016).
707 All the analysed alluvial fans record the uplift and subsequent recycling of the older Hecho Group
708 turbidites (Fig. 14). The overwhelming presence of turbidite pebbles (Fig. 14A-C) in these alluvial
709 fan systems evidences the continuous and high degree of erosion of the flysch basin whose
710 original extent remains unkown as the northern margin of the basin has been eroded (Soler and
711 Puigdefàbregas, 1970). Subordinate clasts found in all the alluvial fans derived from the North
712 Pyrenean Zone (Fig. 14D-F), imply that the drainage area of all the fans extended at least to this
713 northern zone. This gives new insights on the paleodrainage organisation of the Pyrenees, where
714 at least for the west-central segment, the water divide was located further to the north than at
715 the present day (Fig. 14). This is concordant with Babault et al. (2011) who proposed using a
716 geomorphological approach that the water divide migrated from North to South during the
717 Eocene. Moreover, it implies that the North Pyrenean Zone was uncovered or slightly covered
718 by Hecho Group turbidites, so that erosion could recover deeper rocks (mainly Mesozoic and
719 some Paleozoic). It follows that the North Pyrenean Zone could have been the northern border
720 for the Eocene turbiditic basin, or at least a paleohigh created by the early to mid Eocene Lakora-
721 Eaux Chaudes thrust system, with a thin or absent cover of Hecho Group turbidites. This is in
722 agreement with thermochronological data from the North Pyrenean Zone, which indicate
723 cooling since early the Paleogene (Vacherat et al., 2014; Bosch et al., 2016). According to
724 thermochronology, the Axial Zone in the western Pyrenees was deeply buried until the

725 Oligocene (Jolivet et al., 2007; Meresse, 2010; Bosch et al., 2016; Labaume et al., 2016) and,
726 therefore, could not provide Mesozoic or Paleozoic grains during late Eocene-early Oligocene
727 sedimentation in the Jaca basin, thus supporting the North Pyrenean Zone as the main source
728 for these grains.
729 An important feature shown by all the alluvial fans is an increasing content of recycled turbidite
730 fragments (with the exception on the uppermost part of the Canciás fan). We interpret this
731 increase as the record of the development of a new drainage network on the uplifted foreland
732 basin. Activity of the Gavarnie thrust may have generated tectonic disruption of the antecedent
733 fluvial system, causing incision and expansion of the fluvial systems on the uplifted block
734 (basically formed by the turbidites of the Hecho Group), with the subsequent increase of
735 recycled turbidites through time recorded in each of the fans at the outlets (Santa Orosia, Peña
736 Oroel and San Juan de la Peña fans). As such, the alluvial fans are important as a sensitive
737 recorder not only of tectonics and climate (Bull, 1977; Harvey, 1997; Robinson et al., 2005) but
738 also geomorphic system dynamics and landscape response time.
739
740 6. CONCLUSIONS
741
742 A detailed petrological analysis coupling sandstone petrography and clast point counting allows
743 us to define the transition from marine to terrestrial environments in the Jaca foreland basin
744 (Eocene-Oligocene) during a stage characterized by the recycling and closure of the marine
745 basin. Four petrofacies have been identified for the deltaic (Belsué-Atarés Formation) and
746 fluvial-alluvial (Campodarbe Group) systems that are: (i) “Hybrid clast-dominated” petrofacies,
747 (ii) “Carbonatic extrabasinal enriched” petrofacies, (iii) “Siliciclastic dominant” petrofacies, and
748 (iv) “Mixed lithic and carbonatic” petrofacies. The “Hybrid clast-dominated” petrofacies is
749 associated with erosion of the Eocene Hecho Group turbidites (earlier foreland basin deposits),

750 located to the north, whilst the “Siliciclastic dominant” petrofacies is indicative of sediment
751 input from eastern sources, in the central Axial Zone.
752 According to our provenance data, the deltaic systems from the Belsué-Atarés Formation show
753 an interplay between the eastern and the northern sources, highly controlled by growing
754 tectonic structures (Yebra de Basa and Atarés anticlines). Since then, the terrestrial desposits of
755 the Campodarbe Group (Santa Orosia, Canciás, Peña Oroel, and San Juan de la Peña fans) display
756 a dominant and protracted northern source area mainly constituted by the previous turbiditic
757 basin, as evidenced by the high amount of turbiditic pebbles, that can be linked with uplift
758 caused by the Gavarnie thrust. Only minor contributions of distal fluvial siliciclastic rich deposits
759 derived from the central Axial Zone have been observed in the western sector of the basin,
760 evidencing a subordinated axially fed system competing with the large north-derived alluvial
761 fans. Thus, in the Jaca basin the switch between east and north-derived sediments evolved
762 progressively from east to west, consistent with the east to west diachronous character of
763 exhumation of the Pyrenees.
764 We report for first time clasts derived from the North Pyrenean Zone in the alluvial fans of the
765 Jaca basin, being the calcareous flysch and volcanics (Cenomanian-Turonian), black dolostones
766 (Jurassic) and metamorphic-clasts rich breccias (late Cretaceous); the diagnostic lithologies of
767 sediment input from this northern belt of the Pyrenees. Thus, we can infer migration of the main
768 water divide which, during the Eocene-Oligocene, was placed farther north than at present.
769 Moreover, we can infer that the margin of the former turbiditic basin (Hecho Group) was located
770 in that position, as the North Pyrenean Zone had to remain largely uncovered in order to provide
771 Mesozoic and Paleozoic lithologies to the fans.
772 The increase of recycled turbidite clasts from base to top observed in each of the alluvial fans
773 can be interpreted as the sedimentary record of development of a new drainage network on the
774 active pro-wedge. This implies an incision and expansion of the fluvial systems through time and

775 gives new insights of the response of the drainage network to the uplift and topographic growth
776 of the west-central Pyrenees.
777
778 ACKNOWLEDGEMENTS
779
780 This paper is a contribution to the project CGL2014-54180-P, financed by the Ministerio de
781 Economía y Competitividad of Spain. M. Roigé and S. Boya acknowledge support from the
782 Universitat Autònoma de Barcelona (PIF grant). We are very grateful to L. Caracciolo, two
783 anonymous reviewers and the editor J. Knight for their constructive reviews that greatly helped
784 to improve the manuscript. We are indebted to P. Labaume for discussion in the field that has
785 contributed to the development of this work. We would like to thank Conwy Valley Systems
786 Limited to provide us PETROG^{TM} software for compositional data acquisition.
787
788 REFERENCES
789
790 Azambre, B., 1967. Sur les roches intrusives sous-saturées du Crétacé des Pyrénées. Comptes
791 rendus hebdomadaires des séances de l'Académie des sciences 271, 641-3.

792 Babault, J., Van den Driessche, J., Teixell, A., 2011. Retro-to pro-side migration of the main
793 drainage divide in the Pyrenees: geologic and geomorphological evidence. European
794 Geosciences Union General Assembly 13, EGU2011-12567.

795 Barnolas, A., Gil-Pena, I., 2002. Ejemplos de relleno sedimentario multiepisodico en una cuenca
796 de antepais fragmentada: La Cuenca Surpirenaica. Boletín Geológico y Minero de España
797 112, 17–38.

798 Barnolas, A., Teixell, A., 1994. Platform sedimentation and collapse in a carbonate dominated

799 margin of a foreland basin (Jaca basin, Eocene, southern Pyrenees). Geology 22, 1107–
800 1110.

801 Barone, M., Dominici, R., Muto, F., Critelli, S., 2008. Detrital Modes in a Late Miocene Wedge-
802 Top Basin, Northeastern Calabria, Italy: Compositional Record of Wedge-Top Partitioning.
803 Journal of Sedimentary Research 78, 693–711.

804 Bosch, G.V., Teixell, A., Jolivet, M., Labaume, P., Stockli, D., Domènech, M., Monié, P., 2016.
805 Timing of Eocene-Miocene thrust activity in the Western Axial Zone and Chaînons
806 Béarnais (west-central Pyrenees) revealed by multi-method thermochronology. Comptes
807 Rendus Geoscience 348, 246–256.

808 Bull, W.B., 1977. The alluvial-fan environment. Progress in Physical Geography 1, 222–270.

809 Caja, M.A., Marfil, R., Garcia, D., Remacha, E., Morad, S., Mansurbeg, H., Amorosi, A.,
810 Martínez-Calvo, C., Lahoz-Beltrá, R., 2010. Provenance of siliciclastic and hybrid turbiditic
811 arenites of the Eocene Hecho Group, Spanish Pyrenees: Implications for the tectonic
812 evolution of a foreland basin. Basin Research 22, 157–180.

813 Casteras, M., Villanova, M., Godechot, Y., 1970. Carte géologique détaillée de la France a
814 1/50000. Feullie [1052], Lourdes.

815 Chayes, F., 1952. The finer-grained calcalkaline granites of New England. The Journal of
816 Geology 60, 207–254.

817 Comas-Cufí, M., Thió-Henestrosa, S., 2011. CoDaPack 2.0: a stand-alone, multi-platform
818 compositional software. In: Egozcue, J.J., Tolosana-Delgado, R., Ortego, M.I. (Eds.),
819 CoDaWork'11: 4th International Workshop on Compositional Data Analysis. Sant Feliu de
820 Guíxols (http://congress.cimne.com/codawork11/Admin/Files/FilePaper/p28.pdf).

821 Costa, E., Garcés, M., López-Blanco, M., Beamud, E., Gómez-Paccard, M., Larrasoaña, J.C.,

2010. Closing and continentalization of the South Pyrenean foreland basin (NE Spain): Magnetochronological constraints. Basin Research 22, 904–917.

Critelli, S., Ingersoll, R.V., 1995. Interpretation of neovolcanic versus palaeovolcanic sand grains: an example from Miocene deep-marine sandstone of the Topanga Group (Southern California). Sedimentology 42, 783–804.

Debon, F., Enrique, P., Autran, A., 1996. Le plutonisme hercynien des Pyréneés. In: Barnolas, A., Chiron, J.C. (Eds.), Synthèse géologique et géophysique des Pyrénées, vol I. BRGM-ITGE, pp. 361–499.

Di Giulio, A., Ceriani, A., Ghia, E., Zucca, F., 2003. Composition of modern streamsands derived from sedimentary source rocks in a temperate climate (Northern Apennines, Italy). Sedimentary Geology 158, 145–161.

Dickinson, W.R., 1970. Interpreting detrital modes of graywacke and arkose. Journal of Sedimentary Research 40, 695–707.

Dickinson, W.R., 1988. Provenance and sediment dispersal in relation to paleotectonics and paleogeography of sedimentary basins. In: Kleinspehn, K.L., Paola, C. (Eds.), New Perspectives in Basin Analysis. Springer-Verlag, New York, pp. 3–25.

Dickinson, W.R., Beard, L.S., Brakenridge, G.R., Erjavec, J.L., Ferguson, R.C., Inman, K.F., Ryberg, P.T., 1983. Provenance of North American Phanerozoic sandstones in relation to tectonic setting. American Association of Petroleum Geologists Bulletin 94, 222–235.

Dreyer, T., Corregidor, J., Arbues, P., Puigdefabregas, C., 1999. Architecture of the tectonically influenced Sobrarbe deltaic complex in the Ainsa Basin, northern Spain. Sedimentary Geology 127, 127–169.

Dryden, J.A.L., 1931. Accuracy in percentage representation of heavy mineral frequencies.

Proceedings of the National Academy of Sciences of the United States of America 17, 233–238.

Dunham, R.J., 1962. Classification of carbonate rocks according to depositional texture. In: Ham, W.E. (Ed.), Classification of Carbonate Rocks—A Symposium. American Association of Petroleum Geologists Memoir 1, Tulsa, OK, pp. 108 – 121.

Fitzgerald, P.G., Muñoz, J.A., Coney, P.J., Baldwin, S.L., 1999. Asymmetric exhumation across the Pyrenean orogen: Implications for the tectonic evolution of a collisional orogen. Earth and Planetary Science Letters 173, 157–170.

Fontana, D., Zuffa, G.G., Garzanti, E., Pyrenees, C., 1989. The Eocene Hecho Group Turbidite Complex (south-central Pyrenees, Spain). Basin Research 2, 223–237.

Fosdick, J.C., Grove, M., Graham, S.A., Hourigan, J.K., Lovera, O., Romans, B.W., 2015. Detrital thermochronologic record of burial heating and sediment recycling in the Magallanes foreland basin, Patagonian Andes. Basin Research 27, 546-572.

Garzanti, E., Limonta, M., Resentini, A., Bandopadhyay, P.C., Najman, Y., Andò, S., Vezzoli, G., 2013. Sediment recycling at convergent plate margins (Indo-Burman Ranges and Andaman-Nicobar Ridge). Earth-Science Reviews 123, 113–132.

Garzanti, E., Vezzoli, G., 2003. A Classification of Metamorphic Grains in Sands Based on their Composition and Grade. Journal of Sedimentary Research 73, 830–837.

Gazzi, P., 1966. Le arenarie del flysh sopracretaceo dell'Apenino modenese; correlazioni con il flysh Monghidoro. Mineralogica et Petrographica Acta 12, 69–97.

Gómez-Gras, D., Roigé, M., Fondevilla, V., Oms, O., Boya, S., Remacha, E., 2016. Provenance constraints on the Tremp Formation paleogeography (southern Pyrenees): Ebro Massif VS Pyrenees sources. Cretaceous Research 57, 414-427.

868 Graham, S.A., Tolson, R.B., Decelles, P.G., Ingersoll, R.V., Bargar, E., Caldwell, M., Cavazza, W.,
869 Edwards, D.P., Follo, M.F., Handschy, M.F., Lemke, J.F., Moxton, I., Rice, R., Smith, G.A.,
870 White, J., 1986. Provenance modelling as a technique for analysing source terrane
871 evolution and controls on foreland sedimentation. In: Allen, P.A., Homewood, P. (Eds.),
872 Foreland Basins. International Association of Sedimentologists, Special Publication 8, pp.
873 425–436.

874 Harvey, A.M., 1997. The role of alluvial fans in arid zone fluvial systems. In: Thomas, D.S.G.
875 (Ed.), Arid Zone Geomorphology. Wiley, Chichester, pp. 231-259.

876 Hogan, P.J., 1993. Geochronologic, tectonic and stratigraphic evolution of the southwest
877 Pyrenean foreland basin, Northern Spain. PhD thesis, University of Southern California,
878 208pp.

879 Hogan, P.J., Burbank, D.W., 1996. Evolution of the Jaca piggyback basin and emergence of the
880 External Sierra, southern Pyrenees. In: Friend, P.F., Dabrio, C.J. (Eds.), Tertiary Basins of
881 Spain. Cambridge University Press, pp. 153 – 160.

882 Howard, J.L., 1993. The statistics of counting in rudites: a review, with examples from the
883 Upper Palaeogene of southern California, USA. Sedimentology 40, 157–174.

884 Ingersoll, R.V., Bullard, T.F., Ford, R.L., Grimm, J.P., Pickle, J.D., Sares, S.W., 1984. The Effect of
885 Grain Size on Detrital Modes: A Test of the Gazzi-Dickinson Point-Counting Method.
886 Journal of Sedimentary Petrology 54, 103-116.

887 Jolivet, M., Labaume, P., Monié, P., Brunel, M., Arnaud, N., Campani, M., 2007.
888 Thermochronology constraints for the propagation sequence of the south Pyrenean
889 basement thrust system (France-Spain). Tectonics 26, doi:10.1029/2006TC002080.

890 Labaume, P., Meresse, F., Jolivet, M., Teixell, A., Lahfid, A., 2016. Tectono-thermal history of an

exhumed trhust-sheet-top basin: an example from the south Pyrenean thrust belt. Tectonics 35, 1280-1313.

Labaume, P., Mutti, E., Séguret, M., 1987. Megaturbidites: a depositional model from the Eocene of the SW-Pyrenean Foreland Basin, Spain. Geo-Marine Letters 7, 91–101.

Labaume, P., Séguret, M., Seyve, C., 1985. Evolution of a turbiditic foreland basin and analogy with an accretionary prism: Example of the Eocene South-Pyrenean Basin. Tectonics 4, 661–685.

Lagabrielle, Y., Labaume, P., Saint-Blanquat, M., 2010. Mantle exhumation, crustal denudation, and gravity tectonics during Cretaceous rifting in the Pyrenean realm (SW Europe): Insights from the geological setting of the lherzolite bodies. Tectonics 29, doi:10.1029/2009TC002588.

Lith, J.G.J., 1965. Geology of the Spanish part of the Gavarnie nappe (Pyrénées) and its underlying sediments near Bielsa (Provincia of Huesca). Thesis Utrecht, Geologica Ultraiectina 10, 67pp.

Mangin, J.P., 1960. Le Nummulitique Sud-Pyrénéen à l'ouest de l'Aragón. Pirineos 51–58, 79–83.

Marfil, R., 1970. Estudio petrogenético del Keuper en el sector meridional de la Cordillera Ibérica. Estudios Geológicos 2, 113–163.

Marsaglia, K.M., 1992. Petrography and provenance of volcanoclastic sands recovered from the Izu–Bonin Arc, Leg 126. In: Taylor, B., Fujioka, K. (Eds.), Proceedings of the Ocean Drilling Program. Scientific results, 126. Ocean Drilling Program, College Station, Texas, pp. 139–154.

Meresse, F., 2010. Dynamique d'un prisme orogénique intracontinental: évolution

914 thermochronologique (traces de fission sur apatite) et tectonique de la Zone Axiale et des
915 piedmonts des Pyrénées centro- occidentales. Université Montpellier II, Montpellier,
916 France, 277pp.

917 Metcalf, J.R., Fitzgerald, P.G., Baldwin, S.L., Muñoz, J.A., 2009. Thermochronology of a
918 convergent orogen: Constraints on the timing of thrust faulting and subsequent
919 exhumation of the Maladeta Pluton in the Central Pyrenean Axial Zone. Earth and
920 Planetary Science Letters 287, 488–503.

921 Michael, N., 2013. Functioning of an ancient routing system, the Escanilla Formation, South
922 Central Pyrenees. PhD thesis, Imperial College London, 284pp.

923 Mochales, T., Barnolas, A., Pueyo, E.L., Serra-Kiel, J., Casas, A.M., Samsó, J.M., Ramajo, J.,
924 Sanjuán, J., 2012. Chronostratigraphy of the Boltaña anticline and the Ainsa Basin
925 (southern pyrenees). American Association of Petroleum Geologists Bulletin 124, 1229-
926 1250.

927 Montes, M., Colombo, F., 1996. Análisis secuencial y correlación de los abanicos aluviales de
928 Peña Oroel y la Sierra de Cancias (Eoceno superior. Cuenca Surpirenaica Central).
929 Geogaceta 20, 76-79.

930 Mouthereau, F., Filleaudeau, P.Y., Vacherat, A., Pik, A., Lacombe, O., Fellin, M.G., Castelltort,
931 S., Christophoul, F., Masini, E., 2014. Placing limits of shortening evolution in the
932 Pyrenees: role fo margin architecture and implications for the Iberia/Europe
933 convergence. Tectonics 33, 2283–2314.

934 Muñoz, J.A., 1992. Evolution of a continental collision belt: ECORS-Pyrenees crustal balanced
935 cross-section. In: McClay, K.R. (Ed.), Thrust Tectonics. Chapman & Hall, London, U.K., pp.
936 235–246.

937 Mutti, E., 1985. Turbidite systems and their relations to depositional sequences. In: Zuffa, G.G.
938 (Ed.), Provenance of Arenites. NATO ASI Series, Dordrecht, Reidel, pp. 65–93.

939 Nijman, W., Nio, S.D., 1975. The Eocene Montañana Delta (Tremp-Graus Basin, provinces of
940 Lérida and Huesca, Southern Pyrenees, N Spain). Field trip B guidebook (The sedimentary
941 evolution of the Paleogene south Pyrenean Basin). XI International Sedimentological
942 Congress, International Association of Sedimentologists, Nice, Excursion Guidebook, 1-20.

943 Oliva-Urcia, B., Beamud, E., Garces, M., Arenas, C., Soto, R., Pueyo, E.L., Pardo, G., 2015. New
944 magnetostratigraphic dating of the Palaeogene syntectonic sediments of the west-central
945 Pyrenees: tectonostratigraphic implications. In: Pueyo, E.L. (Ed.), Palaeomagnetism in
946 Fold and Thrust Belts: New Perspectives. Geological Society of London, Special
947 Publications 425, pp. 107–128.

948 Oms, O., Dinarès-Turell, J., Remacha, E., 2003. Magnetic stratigraphy from deep clastic
949 turbidites: An example from the Eocene Hecho group (Southern Pyrenees). Studia
950 Geophysica et Geodaetica 47, 275–288.

951 Oms, O., Remacha, E., 1992. Estratigrafía del abanico deltaico de Santa Orosia (Eoceno medio y
952 superior de la cuenca de Jaca, Prov. de Huesca). Geogaceta12, 73-74.

953 Ortí, F., Salvany, J.M., Rosell, L., Pueyo, J.J., Inglés, M., 1986. Evaporitas antiguas (Navarra) y
954 actuales (Los Monearos) de la Cuenca del Ebro. In: Anadón, P., Cabrera, L. (Eds.), Guía de
955 Las Excursiones Del XI Congreso Español de Sedimentologia. Generalitat de Catalunya,
956 Comissió Interdepartamental de Recerca i Innovació Tecnològica (CIRIT), Barcelona, pp.
957 21–24.

958 Orts, D.L., Folguera, A., Encinas, A., Ramos, M., Tobal, J., Ramos, V.A., 2012. Tectonic
959 development of the North Patagonian Andes and their related Miocene foreland basin
960 (41°30'-43°S). Tectonics 31, 1–24.

961 Payros, A., Pujalte, V., Orue-Etxebarria, X., 1999. The South Pyrenean Eocene carbonate
962 megabreccias revisited: New interpretation based on evidence from the Pamplona Basin.
963 Sedimentary Geology 125, 165–194.

964 Puigdefàbregas, C., 1975. La sedimentación molásica en la cuenca de Jaca. Pirineos 104, 1–188.

965 Puigdefàbregas, C., Muñoz, J.A., Verges, J., 1992. Trusting and foreland basin evolution in the
966 Southern Pyrenees. In: McClay, K.R. (Ed.), Thrust Tectonics. Chapman & Hall, Suffolk, pp.
967 247–254.

968 Remacha, E., Oms, O., Coello, J., 1995. he Rapitán turbidite channel and its related eastern
969 levee-overbank deposits, Eocene Hecho group, south-central Pyrenees, Spain. In:
970 Pickering, K.T., Hiscott, R.N., Kenyon, N.H., Ricci Lucchi, F., Smith, R.D.A. (Eds.), Atlas of
971 Deep Water Environments: Architectural Style in Turbidite Systems. Chapman and Hall,
972 London, pp. 145–149.

973 Remacha, E., Picart, J., 1991. El complejo turbidítico de Jaca y el delta de la arenisca de
974 Sabiñánigo. Estratigrafia. Facies y su relación con la tectónica. Libro Guía Excursión nº8, I
975 Congreso Español Del Terciario, Vic. 116pp.

976 Robinson, R.A.J., Spencer, J.Q.G., Strecker, M.R., Richter, A., Alonso, R.N., 2005. Luminescence
977 dating of alluvial fans in intramontane basins of NW Argentina. In: Mather, A. (Ed.),
978 Alluvial Fans: Geomorphology, Sedimentology, Dynamics. Geological Society of London,
979 Special Publications 251, pp. 153–168.

980 Rodríguez-Fernández, L.R., López-Olmedo, F., Oliveira, J.T., Medialdea, T., Terrinha, P., Matas,
981 J., Martín-Serrano, A., Martín-Parra, L.M., Rubio, F., Marín, C., Montes, M., Nozal, F.,
982 2015. Mapa Geológico de la Península Ibérica, Baleares y Canarias a escala 1:1.000.000.
983 Instituto Geológico y Minero de España (IGME), Madrid.

984 Roigé, M., Gómez-Gras, D., Remacha, E., Daza, R., Boya, S., 2016. Tectonic control on sediment
985 sources in the Jaca basin (Middle and Upper Eocene of the South-Central Pyrenees).
986 Comptes Rendus Geosciences 348, 236-245.

987 Roure, F., Choukroune, P., Berastegui, X., Muñoz, J.A., Villien, A., Matheron, P., 1989. ECORS
988 deep seismic data and balanced cross sections: Geometric constrains on the evolution of
989 the Pyrenees. Tectonics 8, 41–50.

990 Rupke, M.A., 1976. Sedimentology of very thick calcarenite-marlstone beds in a flysch
991 succession, Southwestern Pyrenees. Sedimentology 23, 43-65.

992 Schlunegger, F., Mosar, J., 2011. The last erosional stage of the Molasse Basin and the Alps.
993 International Journal of Earth Sciences 100, 1147–1162.

994 Soler, M., Puigdefàbregas, C., 1970. Líneas generales de la geología del Alto Aragón occidental.
995 Pirineos 96, 5-19.

996 Souquet, P., 1967. Le Crétacé Supérieur Sud-Pyrénées en Catalogne, Aragon et Navarra. Thése
997 d'État, Université de Toulouse, 529 pp.

998 Suttner, L.J., 1974. Sedimentary petrographic provinces: An evaluation. In: Ross, C.A. (Ed.),
999 Paleogeographic Provinces and Provinciality. SEPM Special Publication 21, pp. 75–84.

1000 Teixell, A., 1996. The Anso transect of the southern Pyrenees: basement and cover thrust
1001 geometries. Journal of the Geological Society of London 153, 301–310.

1002 Teixell, A., 1998. Crustal structure and orogenic material budget in the west central Pyrenees.
1003 Tectonics 17, 395–406.

1004 Teixell, A., Labaume, P., Lagabrielle, Y., 2016. The crustal evolution of the west-central
1005 Pyrenees revisited: Inferences from a new kinematic scenario. Comptes Rendus
1006 Geosciences 348, 257–267.

1007 Vacherat, A., Mouthereau, F., Pik, R., Bernet, M., Gautheron, C., Masini, E., Le Pourhiet, L.,
1008 Tibari, B., Lahfid, A., 2014. Thermal imprint of rift-related processes in orogens as
1009 recorded in the Pyrenees. Earth and Planetary Science Letters 408, 296–306.

1010 Vergés, J., Fernàndez, M., Martínez, A., 2002. The Pyrenean orogen: pre-, syn-, and post-
1011 collisional evolution. Journal of the Virtual Explorer 8, 57–76.

1012 Zuffa, G.G., 1980. Hybrid arenites: their composition and classification. Journal of Sedimentary
1013 Petrology 50, 21–29.

1014 Zuffa, G.G., 1985. Optical analyses of arenites: influence of methodology on compositional
1015 results. In: Zuffa, G.G. (Ed.), Provenance of Arenites. NATO ASI Series, Reidel, Dordrecht,
1016 pp. 165–189.

1017 Zuffa, G.G., 1987. Unravelling hinterland and offshore palaeogeography from deep-water
1018 arenites. In: Legget, J.K., Zuffa, G.G. (Eds.), Marine Clastic Sedimentology. Concepts and
1019 Case Studies. Graham and Trotman, London, pp. 39–61.

1020

1021

Figure captions

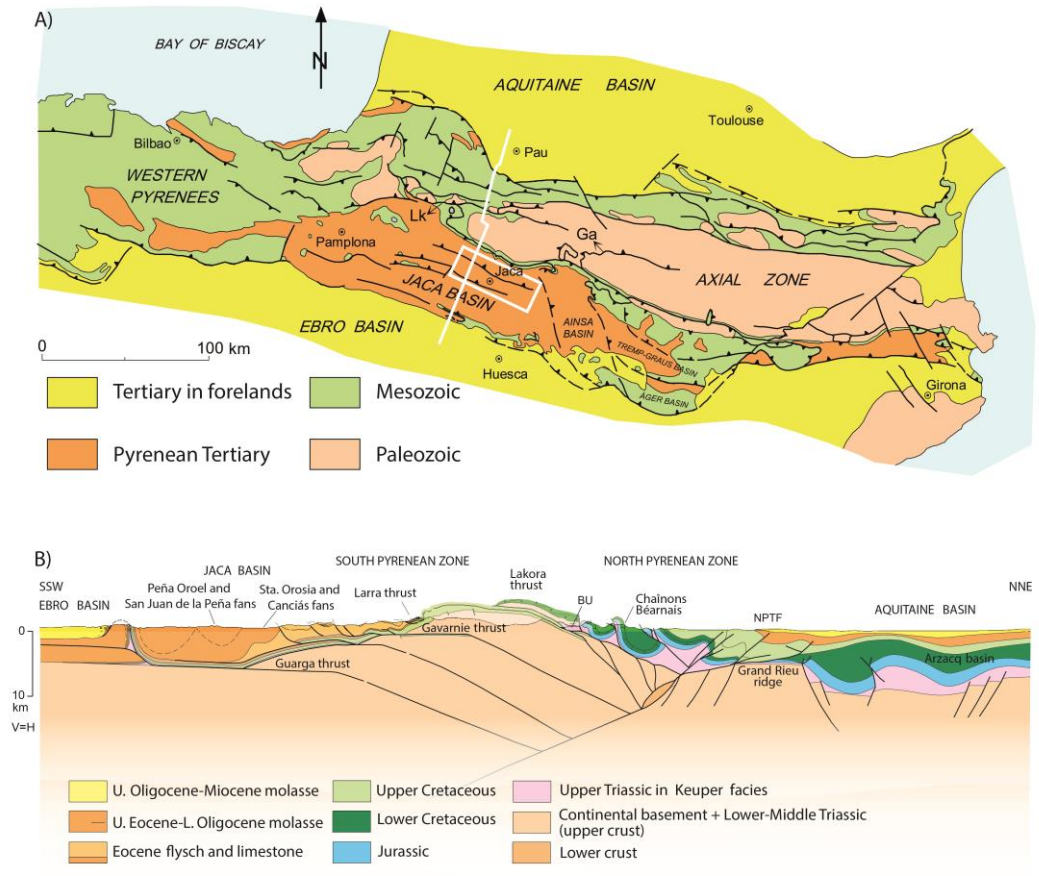

Figure 1. (A) Simplified geological map of the Pyrenees (redrawn from Teixell, 1996), showing the location of the study area (white frame). White line indicates cross-section in Figure 1B. Lk: Lakora thrust; Ga: Gavarnie thrust. (B) Crustal cross-section of the west-central Pyrenees (simplified from Teixell et al., 2016), showing both the South Pyrenean Zone and the North Pyrenean Zone. NPFT: North-Pyrenean Frontal Thrust; BU: Bedous Triassic Unit.

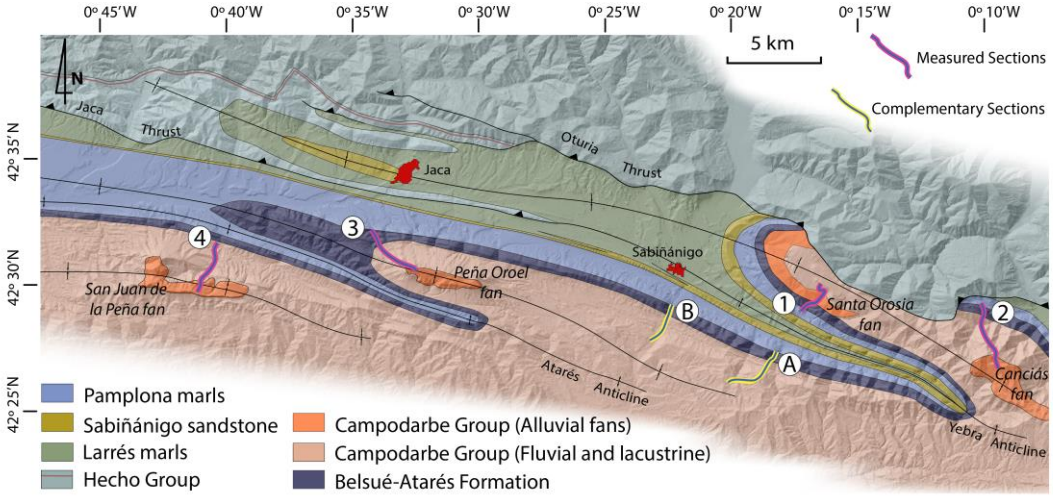

1029

1030 Figure 2. Geological map of the northern sector of the Jaca basin. Red-blue lines show the
1031 location of the four measured sections represented in Figures 7-10. Numbers refer to each
1032 section: (1) Santa Orosia section; (2) Canciás section; (3) Peña Oroel section and (4) San Juan de
1033 la Peña section. Yellow-grey lines are the location of the non-measured but sampled sections
1034 (complementary sections). Letters refer to: (A) Abenilla section and (B) Sabiñánigo section.

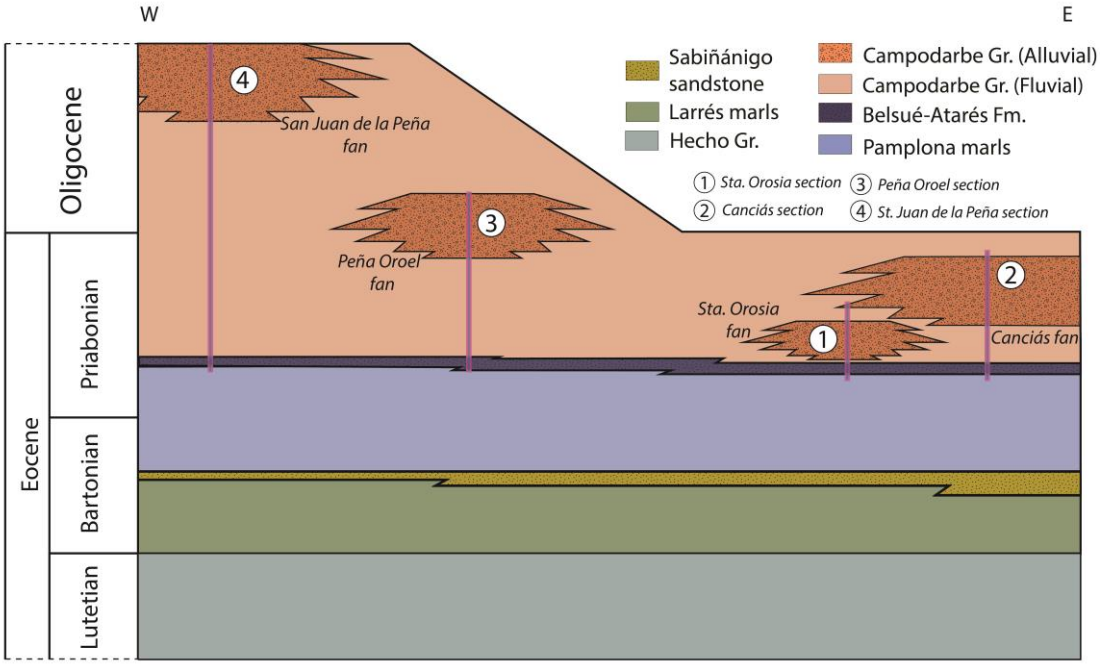

1035

Figure 3. General stratigraphic cross-section sketch summarizing the relationships of the analysed alluvial fans. Stratigraphic ages extracted from Labaume et al. (1985), Hogan and Burbank (1996) and Oms et al. (2003). Blue-purple bars indicate the position of the measured stratigraphic logs.

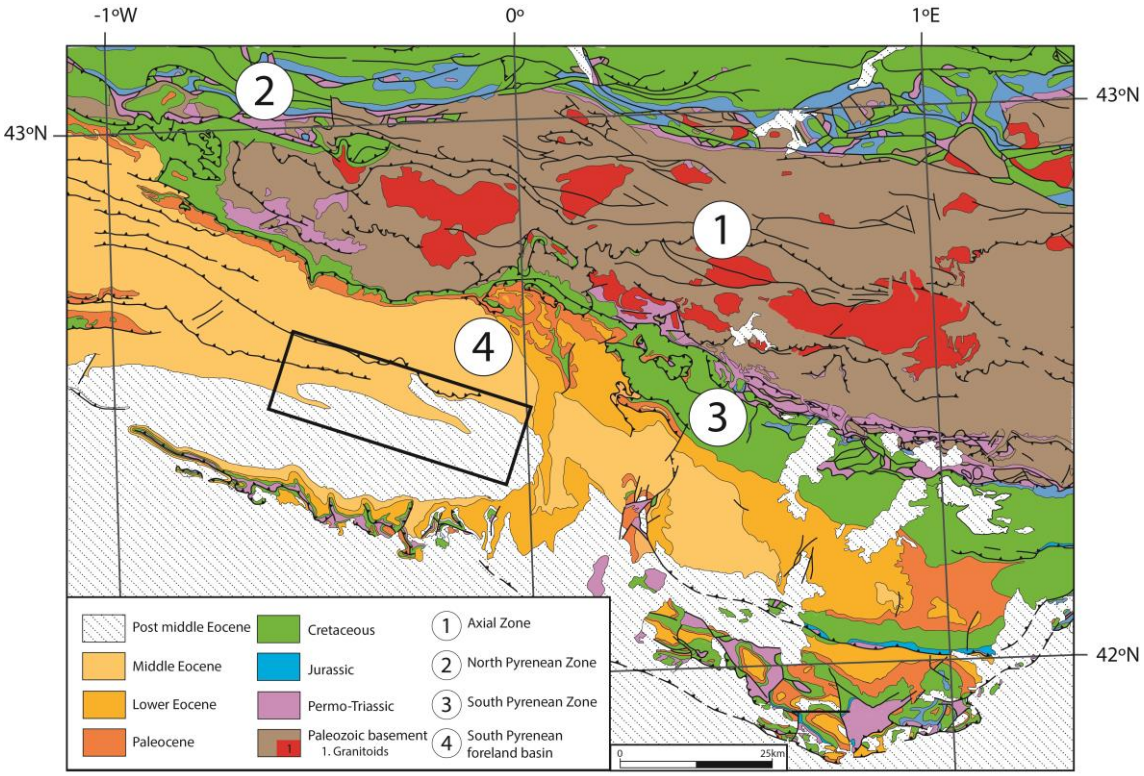

Figure 4. Geological map of the central Pyrenees (modified from a synthesis by Rodríguez-Fernández et al., 2015) showing the potential source rock terrains for the late Eocene-Oligocene systems of the Jaca basin. Dark frame represents the location of the study area.

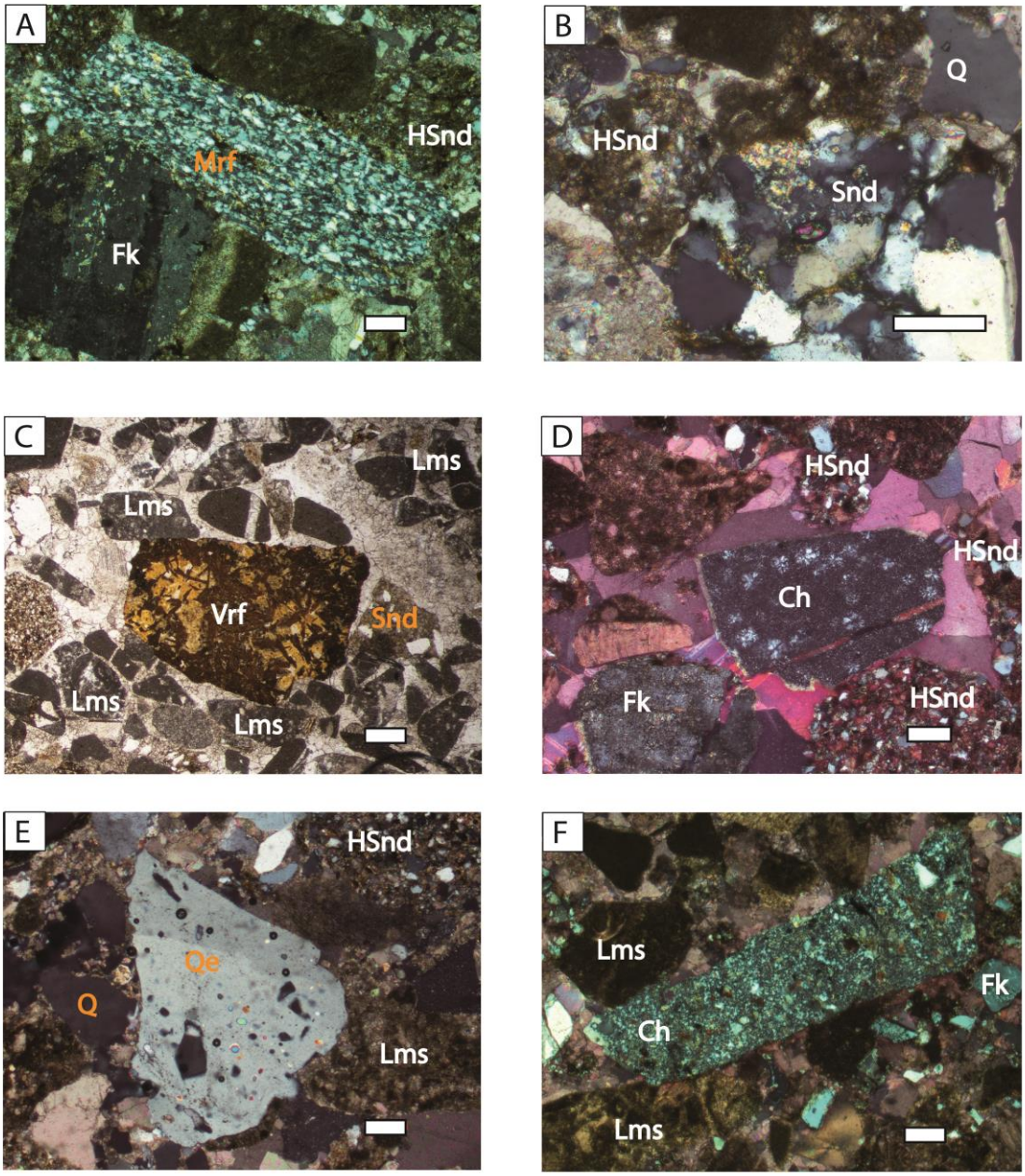

1044

1045 Figure 5. Optical photomicrographs of the main non-carbonate extrabasinal grains. (A) Sample
1046 of the Belsué-Atarés Formation in the Canciás fan: Schist rock fragment (Mrf), feldspar grain
1047 partially replaced (Fk) and hybrid sandstone rock fragment (HSnd) (cross-polarized, XPL); (B)
1048 Sample of the Santa Orosia fan: Hybrid sandstone rock fragment (HSnd), quartz grain (Q) and
1049 quartzarenite rock fragment (Snd) (XPL); (C) Sample of the Canciás fan: Volcanic rock fragments
1050 (Vrf), sandstone rock fragment (Snd) and limestone rock fragments (Lms) (plane polarized,PPL);
1051 (D) Sample of the Santa Orosia fan: Radiolarite rock fragment (Ch), K-feldspar grain (Fk) and

hybrid sandstone rock fragments (HSnd) (XPL); (E) Sample of the Santa Orosia fan: Quartz grain (Q), quartz with evaporitic inclusions (Qe), hybrid sandstone rock fragments (HSnd) and limestone rock fragments (Lms) (XPL); and (F) Sample of the San Juan de la Peña fan: fan: Silicified rock fragment (Ch), feldspar grain (Fk) and limestone rock fragments (Lms) (XPL). The white scale bar is 1 mm.

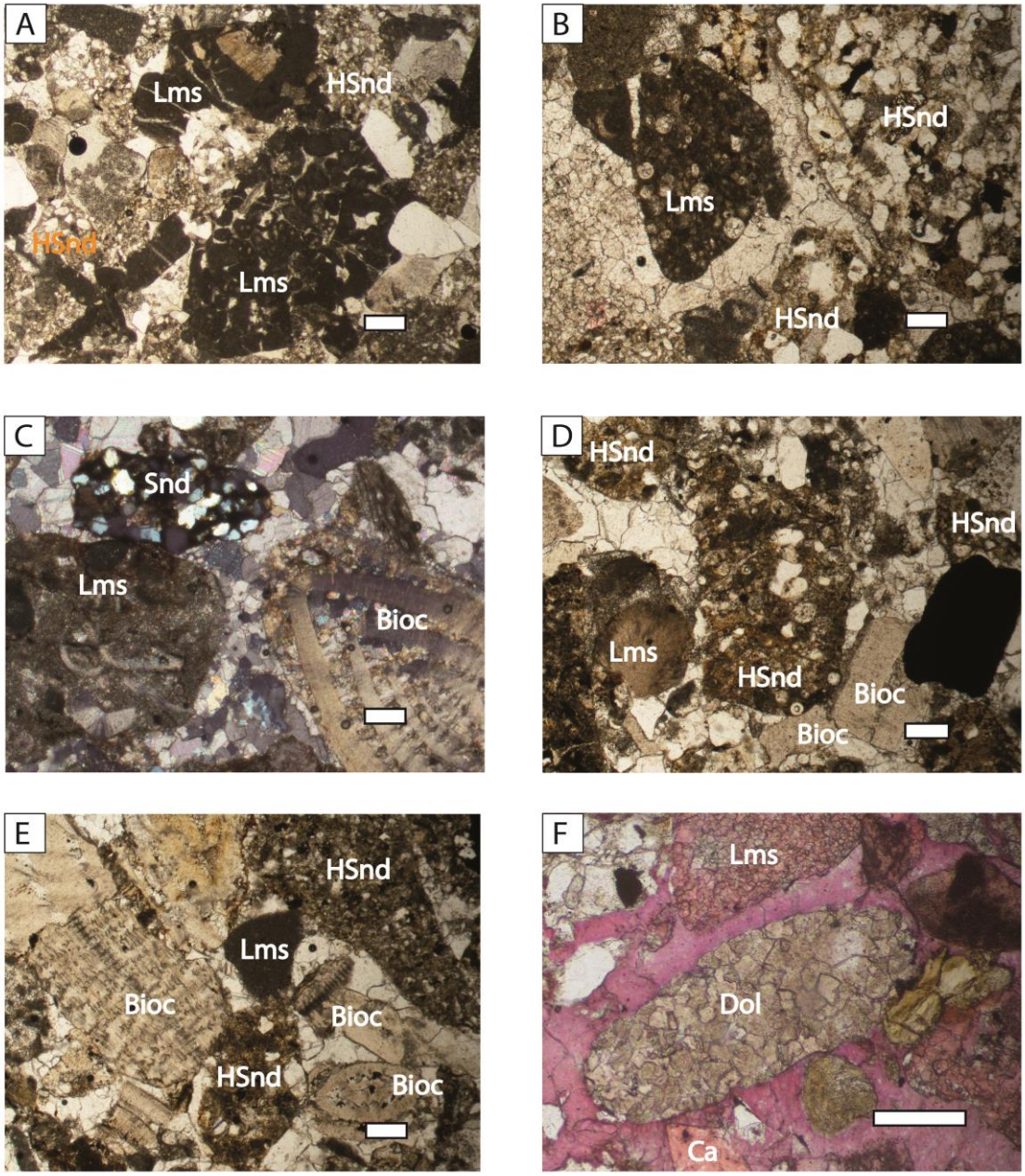

Figure 6. Optical photomicrographs of the main carbonatic extrabasinal grains: (A) Sample of the Canciás fan: Micritic and grainstone limestone fragments (Lms), and hybrid sandstone rock

fragments (HSnd) (PPL); (B) Sample of the Canciás fan: Turonian fossiliferous limestone rock fragment (Lms) and hybrid sandstone rock fragments (HSnd) (PPL); (C) Sample of the San Juan de la Peña fan: fan: Bioclastic limestone rock fragment (Lms), quartzarenite rock fragment (Snd) and a recycled nummullites (Bioc) with inherited cement (XPL); (D) Sample of the Peña Oroel fan: Hybrid sandstone rock fragments (HSnd), limestone rock fragments (Lms) and recycled bioclasts (Bioc) (PPL); (E) Sample of the San Juan de la Peña fan: fan: Hybrid sandstone rock fragments (HSnd), limestone rock fragments (Lms) and recycled bioclasts (Bioc) (PPL); and (F) Sample of the Santa Orosia fan: Crystalline limestone rock fragment (Lms), mono-crystalline calcite (Ca) and dolostone rock fragment with sucrosic texture (Dol) (PPL). The white scale bar is 1 mm.

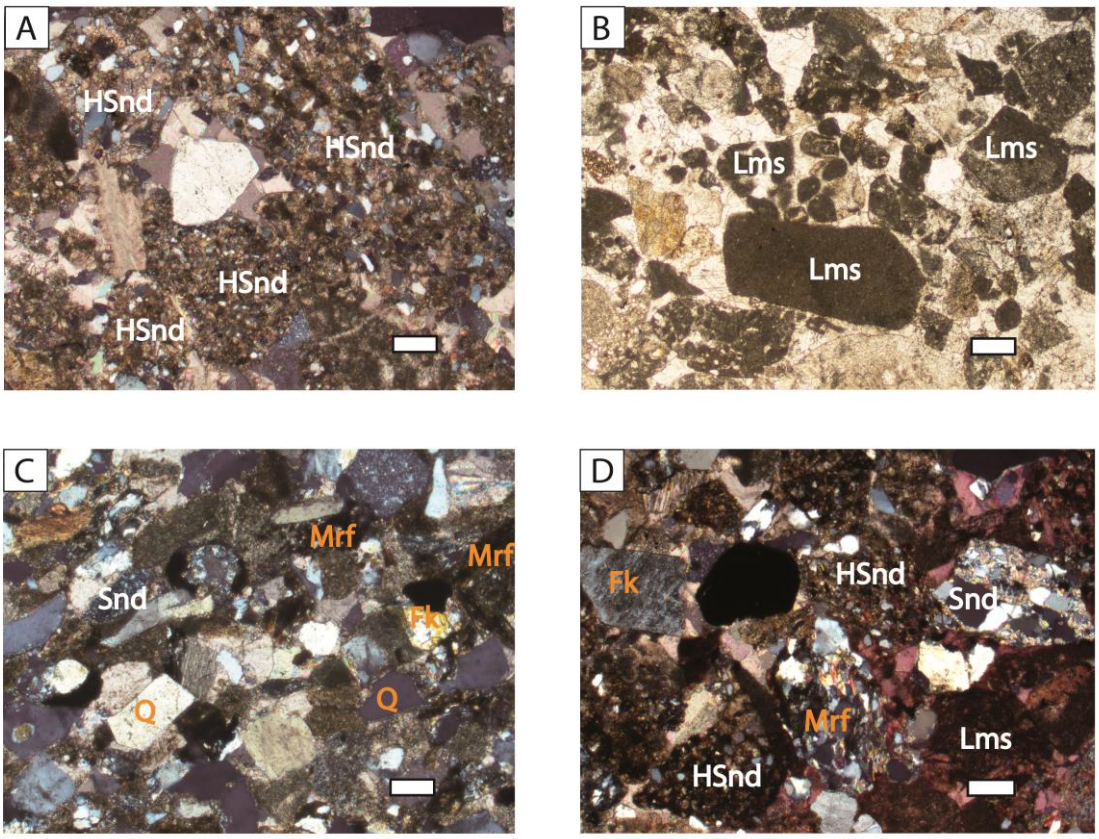

Figure 7. Optical photomicrographs of the described petrofacies: (A) General view of “Hybrid clast-dominated” petrofacies showing the large amount of hybrid sandstone rock fragments (HyS) (XPL); (B) General view of “Carbonate extrabasinal enriched” petrofacies, with abundant

micritic and bioclastic limestone (Lms) fragments and subordinated hybrid sandstone rock fragments (PPL); (C) “Siliciclastic dominant” petrofacies characterized by the higher contents of quartz (Q), metamorphic rock fragments (Mrf) and feldspar grains (Fk), and by the absence of hybrid sandstone rock fragments (XPL); and (D) Appearance of “Mixed lithic and carbonatic” petrofacies, showing the coexistence of hybrid sandstone rock fragments (HSnd) with abundant carbonatic (Lms) and siliciclastic grains such as schists (Mrf) and feldspar grains (Fk) (XPL). The white scale bar is 1 mm.

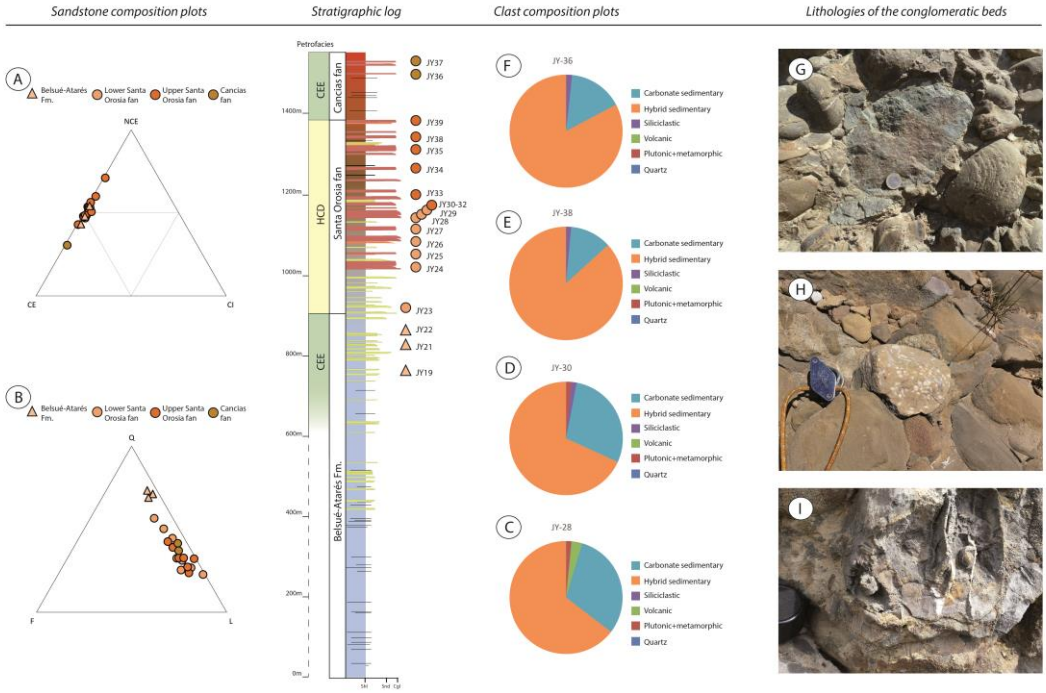

Figure 8. Results for the Santa Orosia section (see location in Fig. 3). The stratigraphic log (modified from Roigé et al., 2016) displays the stratigraphic position of the analysed samples represented in compositional ternary diagrams (A) and (B), and the occurrence of petrofacies (CEE, “Carbonate extrabasinal enriched” petrofacies; HCD, “Hybrid clast-dominated” petrofacies”). (A) First-order compositional plot (Zuffa, 1980) where NCE, Non-Carbonate Extrabasinal grains; CE, Carbonate Extrabasinal; and CI, Carbonate Intrabasinal; (B) QFL compositional plot (Dickinson et al., 1983) where Q, Quartz; F, Feldspar; and L, Lithic fragments.

Clast composition plots (C), (D), (E) and (F) are named according the sample name that coincides with the stratigraphic position were point-counting was perfomed.; From (C) to (F) compositional diagrams of the main clast lithologies in the Santa Orosia (JY28-JY30-JY38) and Canciás alluvial fans (JY36), displaying an increase on the content of hybrid sedimentary clasts toward the top of the Santa Orosia fan; (G) Green dolerite clasts (ophite) surrounded by hybrid sedimentary clasts; (H) Clast of a bioclastic limestone with alveolinids surrounded by hybrid sedimentary clasts; and (I) Grey limestone clast with brachiopods.

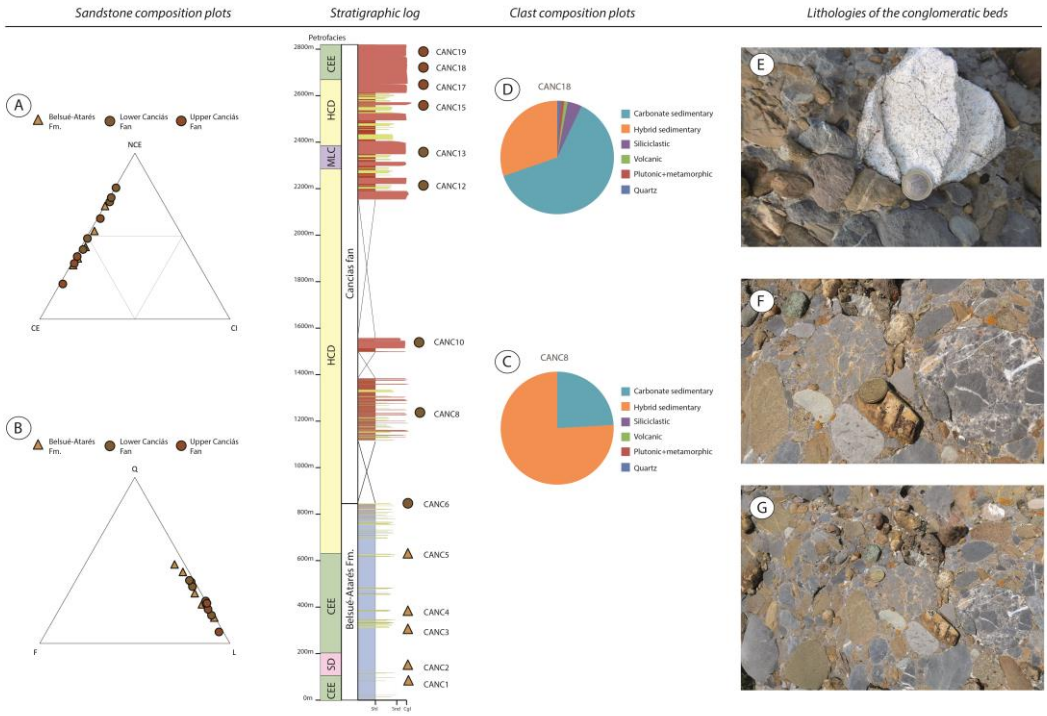

Figure 9. Results for the Canciás section (see location in Fig. 3). The stratigraphic log displays the stratigraphic position of the analysed samples represented in compositional ternary diagrams (A) and (B), and the occurrence of petrofacies (CEE, “Carbonate extrabasinal enriched” petrofacies; SD, “Siliciclastic dominant” petrofacies; MLC, “Mixed lithic and carbonatic” petrofacies; HCD, “Hybrid clast-dominated” petrofacies”). Clast composition plots (C) and (D) are named according the sample name that coincides with the stratigraphic position were point-counting was perfomed. (A) NCE-CE-CI compositional plot, (B) QFL compositional plot (Dickinson

et al., 1983); (C) and (D) compositional diagrams of the main clast lithologies in the Canciás alluvial fan, recording the shift from dominance of hybrid sedimentary clasts (CANC 8) to dominance of limestone clasts (CANC18); (E) White granitic clast (ophite) surrounded by carbonate and hybrid sedimentary clasts, (F) carbonatic breccia clasts (center of the image) and a green dolerite (top left of the image); and (G) dominant proportion of the limestone clasts in the last conglomeratic levels of the Canciás fan.

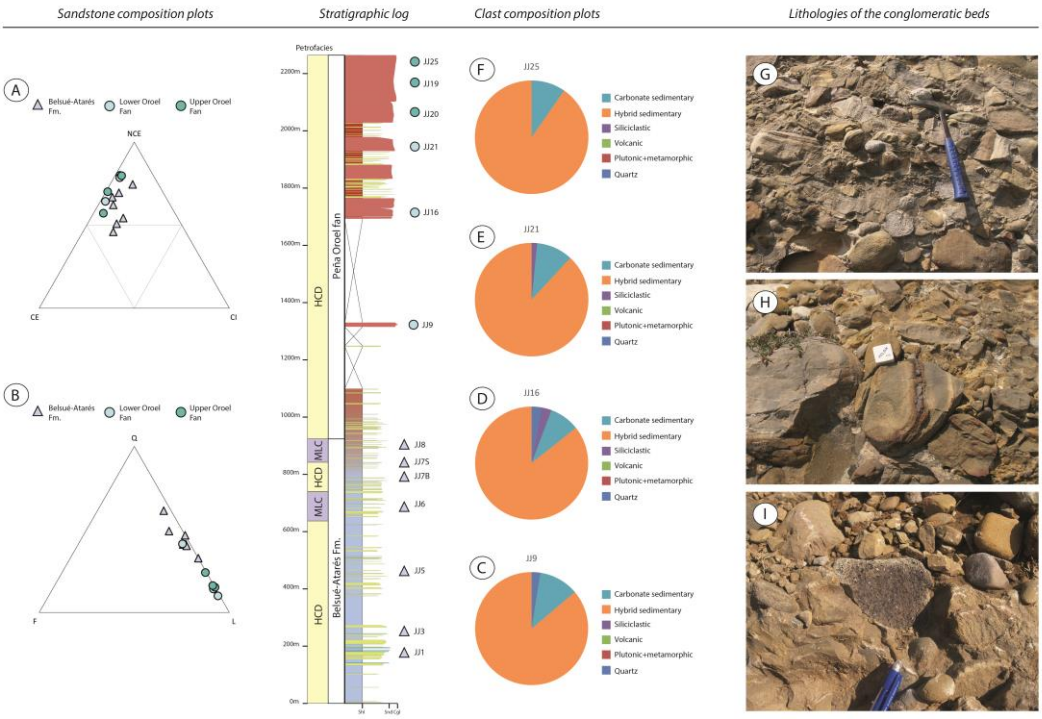

Figure 10. Results for the Peña Oroel section (see location in Fig. 3). The stratigraphic log shows the stratigraphic position of the analysed samples represented in compositional ternary diagrams (A) and (B), and the occurrence of petrofacies (MLC, "Mixed lithic and carbonatic" petrofacies; HCD, "Hybrid clast-dominated" petrofacies). Clast composition plots (C), (D), (E) and (F) are named according the sample name that coincides with the stratigraphic position were point-counting was perfomed. (A) NCE-CE-CI compositional plot; (B) QFL compositional plot (Dickinson et al., 1983); from (C) to (F) compositional diagrams of the main clast lithologies in the Peña Oroel fan (JJ9-JJ16-JJ21-JJ25), recording the high dominance of hybrid sedimentary

clasts; (G) Dominance of hybrid sedimentary clasts (i.e., all the brownish clasts), (H) in the center of the image, a characteristic clast of limestone with black bedded chert; and (I) in the center of the image, a volcanic clast with amygdaloidal texture (black spots are black calcite filling vesicles).

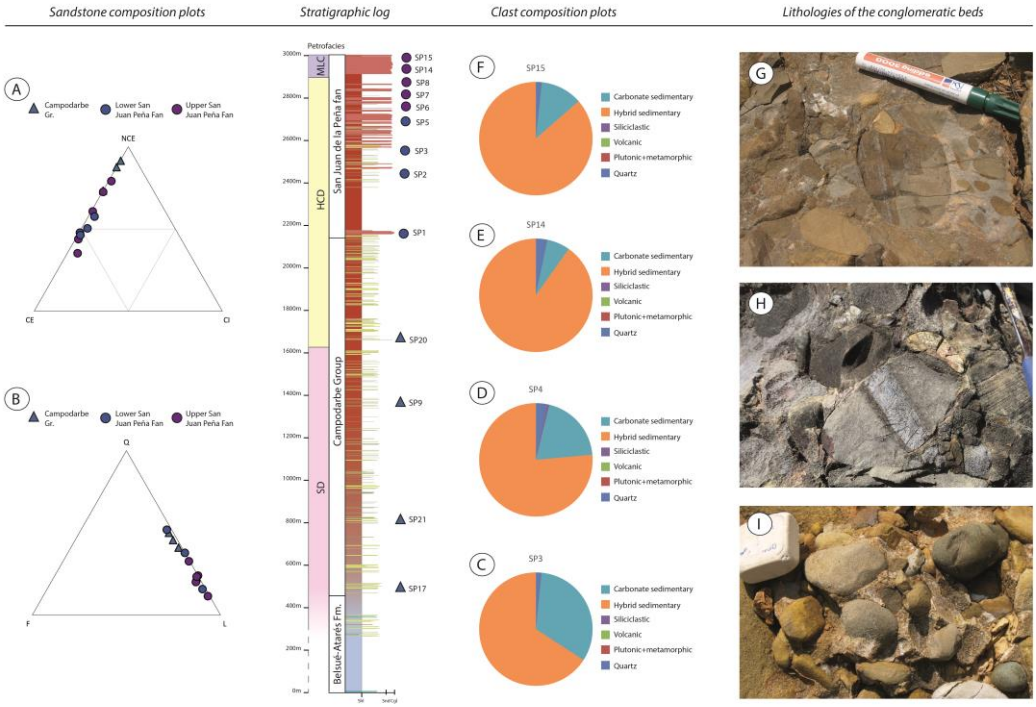

Figure 11. Results for the San Juan de la Peña section (see location in Fig. 3). The stratigraphic log shows the stratigraphic position of the analysed samples represented in compositional ternary diagrams (A) and (B), and the occurrence of petrofacies (SD, "Siliciclastic dominant" petrofacies; MLC, "Mixed lithic and carbonatic" petrofacies; HCD, "Hybrid clast-dominated" petrofacies). Clast composition plots (C), (D), (E) and (F) are named according the sample name that coincides with the stratigraphic position were point-counting was perfomed. (A) NCE-CE-CI compositional plot; (B) QFL compositional plot (Dickinson et al., 1983); from (C) to (F) compositional diagrams of the main clast lithologies in the Peña Oroel fan (JJ9-JJ16-JJ21-JJ25) displaying an increase on the content of hybrid sedimentary clasts towards the top of the San Juan de la Peña fan; (G) in the center of the image, a conglomerate clast, that contains sandstone

and limestone fragments (presumably a clast derived from the erosion of an older late Eocene-Oligocene conglomeratic level); (H) in the center of the image, a clast of limestone with black bedded chert; and (I) in the right side of the image, two green-grey quartzite clasts surrounded by limestone and hybrid sedimentary clasts.

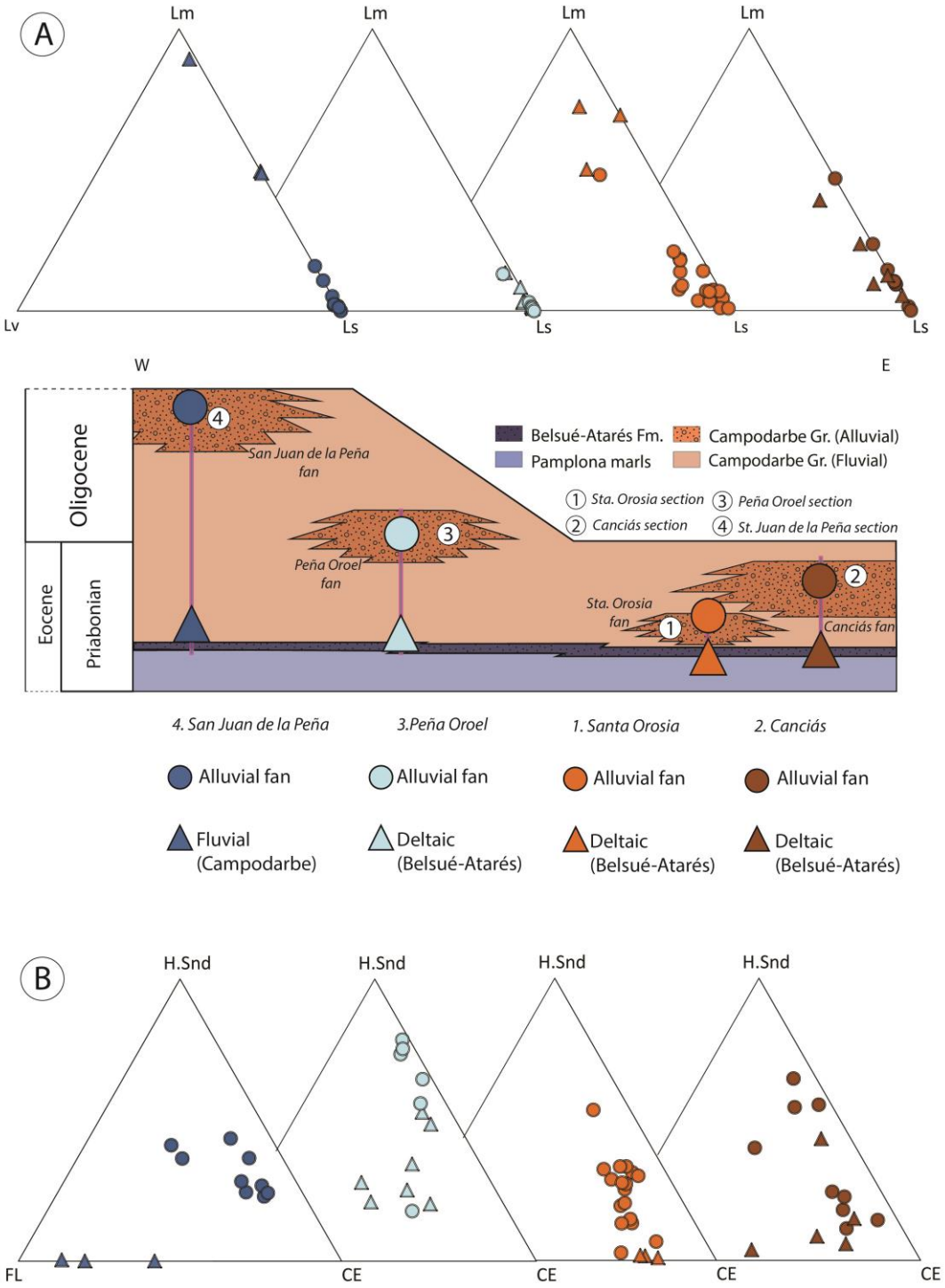

Figure 12. Compositional plots for the Santa Orosia, Canciás, Peña Oroel and San Juan de la Peña sections. Diagrams are arranged according the relative position of each section in the chronostratigraphic chart (from Fig. 3). (A) Third order compositional plots where Lm, Lithic metamorphic grains; Lv, Lithic volcanic grains; and Ls, Lithic sedimentary grains. (B) Fourth order compositional plots where Hybrid Snd, Hybrid sandstone fragments; FL, Feldspar and Lithic grains excluding hybrid sandstone fragments; and CE, Carbonate Extrabasinal grains.

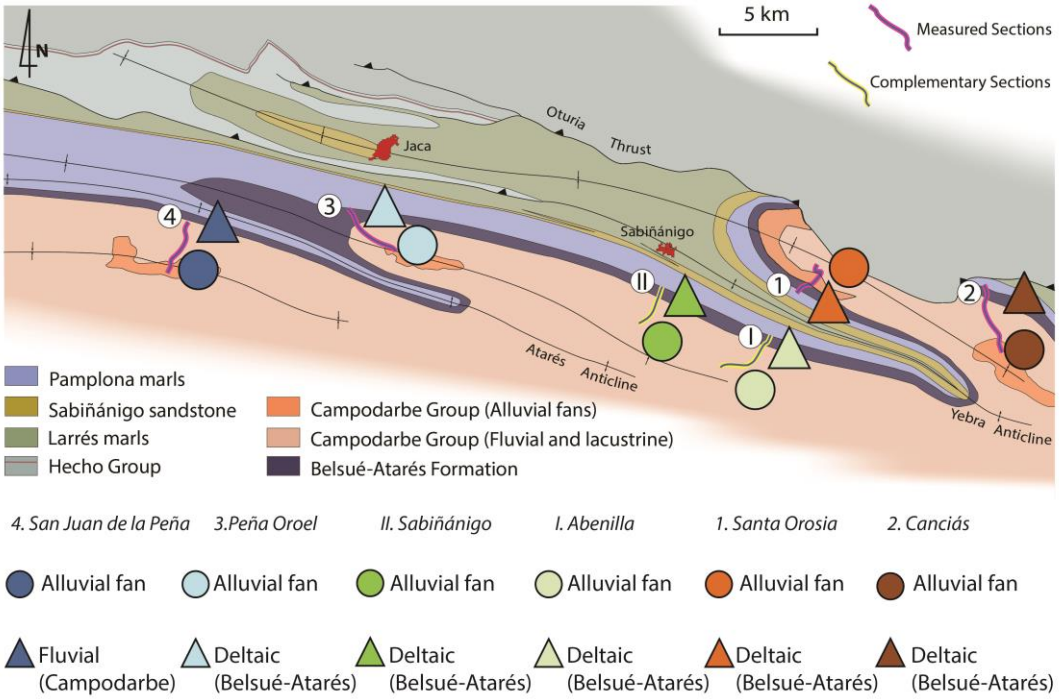

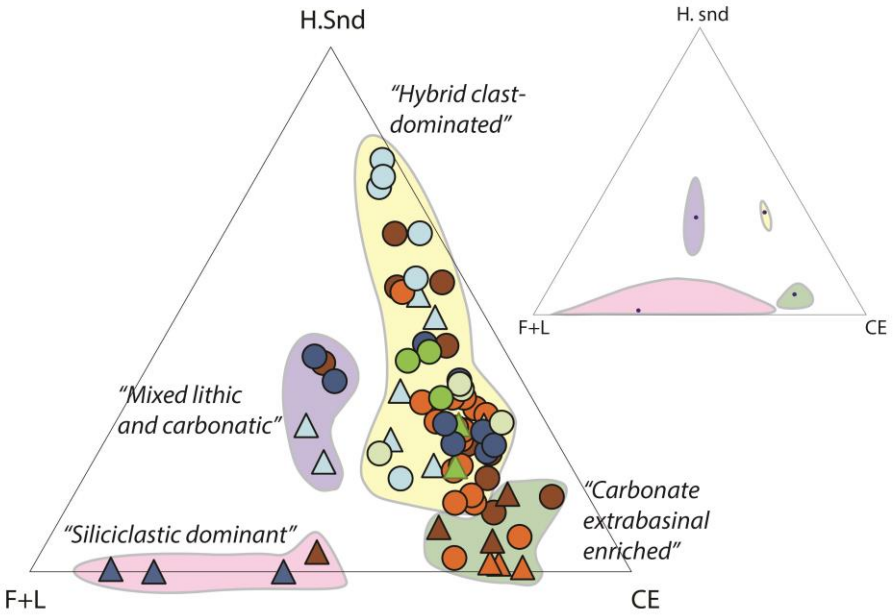

1145

1146 Figure 13. Top: Geological map from Figure 2, with symbols of the sample groups, in order to
1147 facilitate the interpretation of the ternary diagram located below. Bottom: Compositional plot
1148 where Hybrid Snd, Hybrid Sandstone fragments; FL, Feldspar and Lithic grains excluding hybrid
1149 sandstone fragments; and CE, Carbonate Extrabasinal grains. Bottom: Compositional plot

discriminate the four main groups of petrofacies described for all the analysed samples, while the small ternary diagram on the right side shows the mean confidence regions (90%) for each petrofacies. Yellow-coloured fields correspond to “Hybrid clast-dominated” petrofacies, green-coloured fields to “Carbonatic extrabasinal enriched” petrofacies, blue-coloured fields to “Mixed lithic and carbonatic” petrofacies and pink coloured fields to “Siliciclastic dominant” petrofacies.

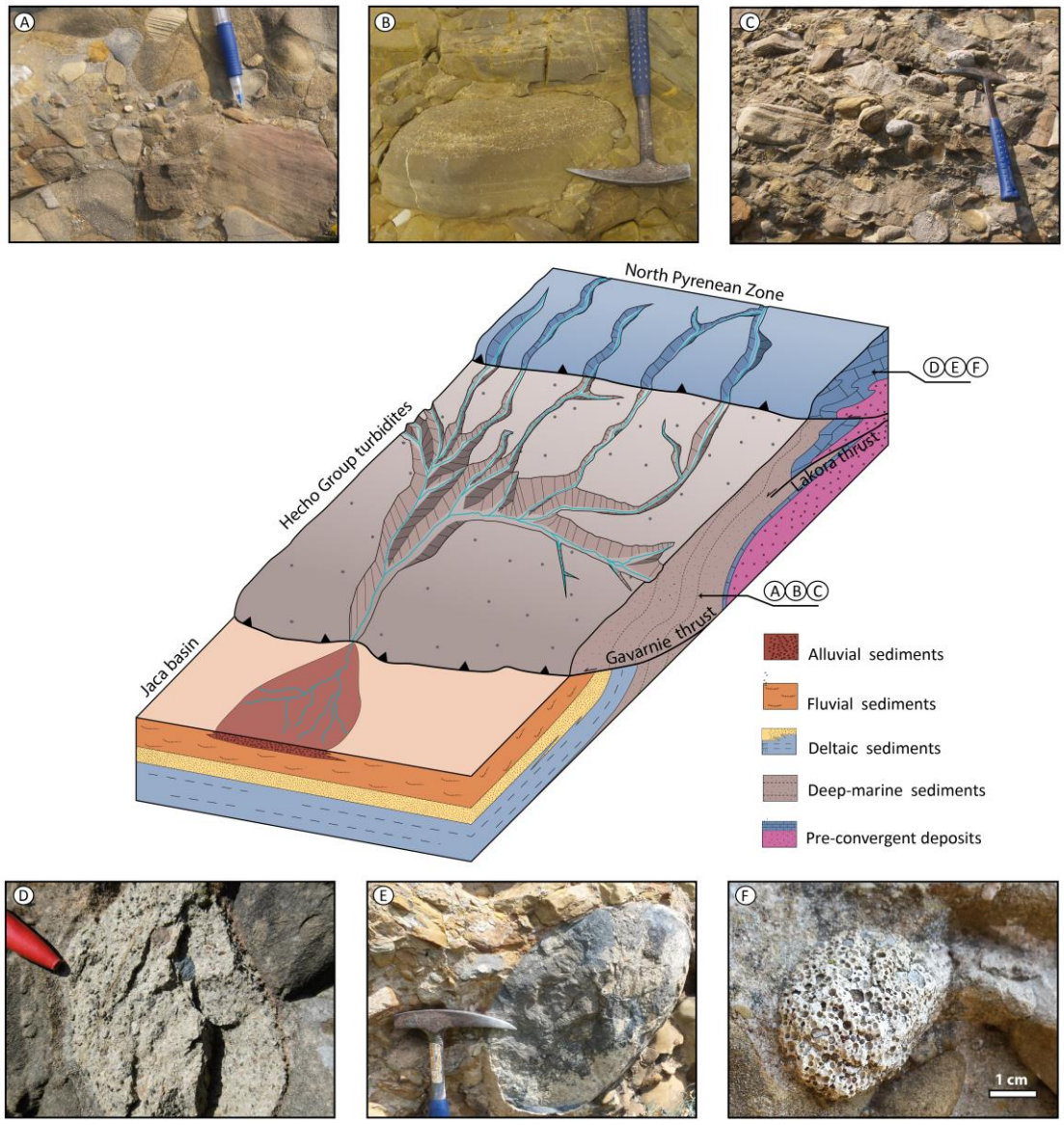

Figure 14. Sketch model for the alluvial fans of the Jaca basin, with images of the diagnostic clasts identifying the nature of the source area. The model applies to any of the northern sourced alluvial fans. A major area of erosion of Hecho Group turbidites results in an increase of

hybrid sandstone fragments in the upper reaches of the alluvial fans. Images (A), (B) and (C) are from clasts that are attributed to erosion of Hecho Group; and are (A) cross-beddings in hybrid arenite clasts; (B) graded hybrid fine-sandstone clasts, and (C) brownish and well-laminated hybrid arenite clasts. Images (D), (E) and (F) are from clasts that are attributed to erosion of the North Pyrenean Zone, and are (D) Ibarrondoa breccia clast; (E) Jurassic black dolostone clast, and (F) Cretaceous amygdaloidal volcanic clast.

Supplementary data

Table 1. Sandstone compositional data (point counting analyses).

Table 2. Clast compositional data (point counting on clasts).